Mass balance and hydrological modeling of the Hardangerjøkulen ice cap in south-central Norway

Trude Eidhammer[1], Adam Booth[2], Sven Decker[3], Lu Li[4], Michael Barlage[1], David Gochis[1], Roy Rasmussen[1], Kjetil Melvold[5], Atle Nesje[6], Stefan Sobolowski[4]

[1]National Center for Atmospheric Research, P.O. Box 3000, Boulder, CO 80307, USA
[2]School of Earth and Environment, University of Leeds, UK
[3]Department of Geoscience, University of Oslo, Norway
[4]NORCE Norwegian Research Centre, Bjerknes Centre for Climate Research, Bergen, Norway
[5]Norwegian Water Resource and Energy Directorate, Oslo, Norway
[6]Department of Earth Science, University of Bergen, Norway

Correspondence to: Trude Eidhammer (trude@ucar.edu)

Abstract.

A detailed, physically based one dimensional, column snowpack model (Crocus) has been incorporated into the hydrological model WRF-Hydro. This allows for direct surface mass balance simulation of glaciers and subsequent modeling of meltwater discharge from glaciers. To evaluate the new system (WRF-Hydro/Glacier), WRF model simulations were downscaled to 1 km grid spacing to provide meteorological forcing data to the WRF-Hydro/Glacier system at 100 m grid spacing. Evaluation of the WRF downscaling showed that it compared well with in situ meteorological observations for most of the simulation period. The WRF-Hydro/Glacier system reproduced the glacier surface winter/summer and net mass balance, snow depth, surface albedo and glacier runoff well compared to observations. The WRF-Hydro/Glacier system is only activated over a priori designated glacier areas. This glacier area is initialized with observed glacier thickness and assumed to be pure ice (with corresponding ice density). This allows for melt of the glacier to continue after all accumulated snow has melted. Furthermore, the simulation of surface albedo over the glacier is more realistic as surface albedo is represented by snow where there is accumulated snow, and glacier ice when all accumulated snow is melted. The improved estimation of albedo has an appreciable impact on the discharge from the glacier during late summer. We have shown that the integrated snow pack system allows for improved glacier surface mass balance studies as well as hydrological studies.

1 Introduction

Glaciers provide natural storage of water supply to rivers. In Norway, these rivers can then contribute water for domestic and industrial consumption, irrigation and hydropower (Sorg et al., 2012; Laghari, 2013, Kaser et al., 2010). Glaciers are among the first indicators of climate variability and change, and thus glacier retreat and changes and associated streamflow effects can impact human water supplies depending on the modifications to glacier melt timing and amount (Immerzeel et al., 2013;

Bolch et al., 2012). It is imperative to understand how glaciers and associated hydrological processes respond to a changing climate to better inform communities that rely on glaciers for their livelihoods and well-being.

35   It is the surface mass balance on glaciers that impacts the subsequent glacier-fed streamflow. Mass balance changes on glaciers in Norway are largely controlled by accumulation-season precipitation and ablation season temperature. This was determined by comparing measured glacier mass balance from stake measurements with meteorological station data (winter precipitation and summer temperature (e.g. Andreassen and Winsvold, 2012). However, elevation gradients and complex topography in many glaciated regions lead to large variations in temperature, precipitation and winds (and thereby transport and deposition

40   of dry snow during the accumulation season) and net radiative exchange across the glacier. Therefore, the proper simulation of the non-homogenous, non-stationary evolution of a glacier requires atmospheric processes at much finer resolution than typical global or regional climate models can provide (i.e. Collier et al., 2013).

Obtaining distributed meteorological forcing data of temperature, precipitation and wind is complicated by the spatial and temporal scarcity of observations, topographic complexity, and by the coarseness of the atmospheric models used for

45   downscaling. As a result, there are major gaps in our knowledge regarding the behavior of glaciers at local to regional scales and the processes that control their variability (Immerzeel et al., 2010; Bolch et al., 2012). Several studies have used dynamical downscaling of regional climate models, on the order of 10-18 km (e.g. Machguth et al., 2009; Kotlarski et al., 2010; Van Pelt et al., 2012). However, they still do not resolve many sub-grid processes and the studies have therefore required statistical corrections to the downscaling. Recently, several studies applied much higher resolution (0.5-2.5 km) regional climate models

50   to provide the heterogeneous forcing required over glaciers (Collier et al., 2013, Molg and Kaser 2011, Bonekamp et al, 2019, Vionnet et al., 2019). Indeed, Lundquist et al. (2020) argue that in many instances in mountain terrain, high-resolution atmospheric models produce better estimates of annual precipitation than the information we can gain from observation networks.

These regional 'atmosphere-only' models typically do not have detailed information about runoff routing processes, which are

55   important components in the glacier hydrological cycle. Glacier melt contributes to discharge, especially during summer when the magnitude of the summer peak river flow often depends on the contribution of melt water from snow and ice to the total river flow. This contribution from glaciers to total flow plays a key role in the glacier-fed rivers in populated regions in Norway in which summer flows are crucial for irrigation, human consumption and energy production. There are now a few regional earth system modelling systems that link an atmospheric regional scale model to a detailed hydrological model - the Weather

60   and Research Forecasting - Hydro (WRF-Hydro) modelling system is one of these (Gochis et al., 2015; Senatore et al., 2015; Arnault et al., 2018; Fersch et al., 2019; Rummler et al., 2019). However, WRF-Hydro does not explicitly include glaciers within the model system, which results in a large uncertainty and underestimation of discharge during the melt season in glacial fed areas like the Himalaya (Li et al., 2017), and parts of the Andes, Scandinavia and North America. The Noah multi-parameterization (Noah-MP, Niu et al., 2011) land surface model (LSM) is often used in the existing WRF-Hydro system,

65   which includes only a glacier land surface category. When snow is accumulated, Noah-MP uses a three-layer snow model to represent the evolution of the snow pack. However, when the seasonal accumulated snow melts off in the summer, the underlying surface is assumed to be old snow (snow packed glacier), while not allowing for areas of bare ice. Furthermore, the underlying ice (glacier) will not melt, as the ice is represented as a surface land cover category.

    By linking a surface mass balance glacier model to the WRF-Hydro system that interacts with the underlying land-
70   surface/hydrological components, the coupled interactions between the energy, water and mass balance budgets over glaciated river basins can be better depicted for projecting future impacts. For this purpose, we chose the Crocus snow model as our starting point to build the system WRF-Hydro/Glacier. Crocus is a one-dimensional, column energy and mass model of snow and ice cover, that uses meteorological conditions as input data and was initially developed for operational avalanche forecasting and simulation of Alpine snow (Brun et al., 1989, 1992). It is a physically-based model, in which the snow depth
75   can be divided into a maximum of 50 layers. A principal strength of the model is the detailed description of the metamorphism process for different types of snow, which allows for a more accurate calculation of snow surface albedo. The model also has a comparatively sophisticated treatment of liquid water retention within the snow/ice matrix compared to snow schemes typically found in land surface models used in weather and climate modelling. The Crocus model was recently used for glacier surface mass balance studies within the French Surfex model by Revuelto et al. (2018) and Vionnet et al. (2019).

80   Norway is home to some of the best-observed glaciers in the world. Its National Water Resource and Energy Directorate (NVE), regularly monitors and assesses the mass balance and length changes of Norwegian glaciers. This paper will focus on the Hardangerjøkulen ice cap, located in south-central Norway. Hardangerjøkulen is the sixth largest glacier on the mainland of Norway, and is located at the main water divide between eastern and western Norway. The glacier covers an area of approximately 71 km² and the highest point on the glacier is 1,863 m a.s.l. (Andreassen and Winsvold, 2012).
85   Hardangerjøkulen is a plateau glacier and has several outlet glaciers, of which Blåisen (not shown) and Midtdalsbreen facing east/northeast and Rembesdalskåka in the west are the best known (Fig. 1). The ice cap has a volume of about 10.64 km3, and the mean ice thickness is about 150 meters with maximum ice thickness of more than 380 m (Melvold et al., 2011).

    In this paper we present the WRF-Hydro/Glacier system in which Crocus is coupled to the WRF Hydro model, with the Crocus model representing the glacier. In section 2 we explain the Crocus implementation while in section 3 we describe the
90   experimental design and forcing evaluation and in section 4 observational data are discussed. The results are presented in section 5 and finally, conclusions and future work are included in section 6.

2 Crocus Implementation

Crocus is an energy and mass-transfer snowpack model, specifically developed for avalanche forecasting (Brun et al., 1989;
95   1992). In this work we use the version that was implemented into the French Surfex model V8.0 (Vionnet et al., 2012). This
version has several updates from older versions of Crocus, such as impacts of wind-drift.

The Crocus snowpack model is a multilayered physically-based snow model that explicitly calculates snow grain properties
in each snow layer and how these properties change over time. The grain properties of dendricity, sphericity and size are
prognosed in Crocus through metamorphosis, compaction and impacts of wind drift and the age of the snow. Furthermore, the
100 snow albedo is calculated based on the snow grain properties from the top 3 cm of the snowpack (Vionett et al., 2012) and is
calculated in three spectral bands (0.3-0.8, 0.8-1.5 and 1.5-2.5 μm). Due to the prognostic calculation of snow grain properties,
Crocus can represent a surface layer consisting of either snow or ice.

In the Crocus model, it is possible to divide the snow into 50 dynamically evolving layers. As new snow is accumulated, a
new active layer is added. As different snow layers become similar (based upon the number of user-set layers, the thickness of
105 the snow layers and the snow grain characteristics), these snow layers will merge into single snow layers.

The Crocus module is added to the Noah MP land surface model to act as a glacier mass balance model. Over designated
glacier grid points, the Crocus snow model represents both snow and ice, while outside of the designated glacier grid points,
the regular three-layer snow model in Noah-MP is used.

Since the current Crocus implementation in WRF-Hydro only acts over designated glacier grid points, we follow Gerbaux et
110 al. (2005), and assume that the temperature at the bottom of the glacier and the ground below are both at 0 ºC, and no fluxes
of heat pass between the glacier bottom and the ground below (i.e. a constant-temperature boundary condition). Importantly,
the Crocus model interacts with the atmosphere by providing fluxes between the surface of the glacier and the atmosphere.
These fluxes are total absorbed solar radiation, total reflected solar radiation, total net longwave radiation, total sensible heat,
evaporation heat flux (and rate) from snow, and ground heat flux. Some diagnostic outputs, such as the 2m temperature and
115 2m vapor mixing ratio are calculated by the original Noah-MP snow model, but with the snow information (snow surface
temperature and albedo) provided by Crocus.

Both Crocus and Noah-MP (for the non-glacier grid points) output runoff from snowmelt (and precipitation). This runoff is
provided to the terrain routing models in the hydrological model system WRF-Hydro. WRF-Hydro is a model-coupling
framework designed to link multiscale process models of the atmosphere and terrestrial hydrology (Gochis et al., 2015; Yucel
120 et al., 2015). In coupled mode it includes the full functionality of the atmospheric Weather Research and Forecasting (WRF)
modelling system. WRF-Hydro enables simulation of land surface hydrology and energy states and fluxes at high spatial
resolutions (typically 1 km or less) using a variety of physics-based and conceptual approaches (Yucel et al., 2015; Senatore

et al., 2015). It contains horizontal routing processes and water management modules and is linked to the Noah-MP land surface module (among others). The added capability of running Crocus as a glacier mass balance module in WRF-Hydro is
125 called the "WRF-Hydro/Glacier" system from here onward.

One of the main reasons to use Crocus for glacier mass balance modeling and the subsequent streamflow modeling is its use of physical parameterization and ease of implementing non-flowing glacier (ice) layers. By comparison, the Noah-MP has only a maximum of three-layers in its snow pack, depending on the total snow depth (Niu et al., 2011). In Noah-MP, the snow albedo option used in this study is calculated based on the snow age through an empirical function. Noah-MP has its own
130 glacier module with the effect that when there is snow, the Noah MP snow module is active and albedo is represented by the Noah-MP 3-layer snow model, and the minimum albedo of snow is set to 0.55. However, when all snow has melted, the surface is represented by the bare glacier land surface category which has an albedo of 0.675 (0.8 in the visible and 0.55 in the near infrared spectral bands) and roughness lengths and heat conductivity typical for glaciers with old snow. Furthermore, this exposed glacier ice cannot melt as the glacier is only a land surface category, and any potential bare ice is not represented with
135 the albedo and roughness lengths representing ice but of old snow. Finally, as a result of these limitations in the Noah-MP glacier formulation, the glacier cannot decrease in mass and extent.

Note that our implementation of Crocus as glacier mass balance model does not address glacier movement (i.e. plastic flow) nor lateral wind (re)distribution of snow. Being a relatively flat dome glacier, the Hardangerjøkulen glacier that we focus on here does not move much in a year, and therefore the lack of dynamical movement of the glacier is not expected to have a
140 major impact on the results in this paper, as we only consider four simulation years. On the other hand, the lateral snowdrift and wind-driven redistribution of snow on Hardangerjøkulen can be significant, and our results are likely impacted by the lack of this physical process in the model. It is worth mentioning that including lateral movement of snow due to snowdrift in the model system is not a trivial task, and is therefore not currently included.

2.1 Initialization of glacier module in WRF-Hydro/Glacier

145 To run the WRF-Hydro/Glacier system, the glacier to be evaluated must be initialized with its thickness and extent. Here we focus on the Hardangerjøkulen; its extent and height were obtained from the NVE (Melvold et al., 2011). Figure 1 shows the glacier thickness and extent of Hardangerjøkulen at 100 m grid spacing (for which the entire WRF-Hydro/Glacier model is run). At initialization, it is assumed that the glacier consists of only ice, and the density is that of pure ice (900 kg/m3). In the simulations presented here, the user-defined maximum layers are set to 40 layers, and the glacier is initialized with all the
150 layers having the same assumed density and snow grain properties. As new snow accumulates during the simulations, the layers representing the glacier will start to merge since all 40 layers are occupied with the initialized ice. Revuelto et al. (2018) also used Crocus for surface mass balance studies. They initialized their glacier with the same glacier thickness (40 m) over the entire glacier and in the six lowest layers with the thickness progressively increasing with depth. In contrast to this study,

they reinitialized the glacier to 40 m every new season (August 1) so that the glacier would not decrease in extent, while here
155   the glacier is only initialized once at the beginning of the simulation with the observed glacier thickness.

As implemented, if the glacier completely melts over a user defined glacier grid point, the original Noah-MP module is used
from this point on. Therefore, as currently implemented, the glacier cannot grow horizontally in extent, it can only decrease in
extent, as no dynamic response of the ice mass is included in the model. Over short model time periods, the lack of increase
in glacier extent might impact a few grid points at the edges of the glacier. However, given the expected increase in temperature
160   in the future we do not expect that limiting glacier horizontal growth will have a major impact over most studied glaciers as
most are likely to decrease in mass and extent.

In Crocus, there are two options to include impacts on the snow due to wind. One of the options impacts the snow density
during blowing snow events (Brun et al., 1997). This option is important in polar environment (Brun et al., 1997), and we
found it necessary in our simulations as well. The other option is the sublimation due to snow drift, which was implemented
165   by Vionnet et al. (2012) and which is in the Crocus version that is used in this study. This option was also crucial to include in
order to accurately simulate the glacier mass balance over Hardangerjøkulen. It is especially important for reproduction of the
observed heterogeneous snow distribution.

3 Experimental Description

For meteorological input data to the WRF-Hydro/Glacier system, dynamically downscaled data from the WRF model version
170   3.9 (Skamarock et al., 2008) was created over Southern Norway. WRF was run with an outer domain (Domain1) with a 3 km
grid spacing and an inner domain (Domain 2) with a 1 km grid spacing (see Fig. 2, top) with 51 stretched vertical levels. The
ECMWF Re-Analysis Interim (ERA-I) dataset was used for input and boundary conditions and the model was run from August
1, 2014 to January 1, 2019. The microphysics scheme used was the Thompson-Eidhammer aerosol aware scheme (Thompson
and Eidhammer, 2014), the Yonsei University (YSU, Hong et al., 2006) scheme for the boundary layer (Hong et al., 2006),
175   the rapid radiative transfer model (RRTMG) for longwave and shortwave radiation calculations (Iacono et al., 2008), and the
Noah-MP land surface model (Niu et al., 2011).

We did not use any lake models, thus, in WRF, the skin temperature of lakes is typically set to the same temperature as the
nearest grid point that is defined as sea surface. With this setting, the lakes will not reach freezing temperatures since the
oceans surrounding southern Norway typically do not freeze in the winter. To rectify this problem, we assign a 10-day moving

180 average skin temperature from the associated ERA-Interim grid point onto the lake grid points to allow a representation of freezing lakes. The fjords still use the sea surface temperature from ERA-Interim.

The 1 km WRF (inner-nest) simulation results are used as input to run WRF-Hydro/Glacier. The WRF-Hydro/Glacier domain has 100 m grid spacing (Fig. 2, bottom) and covers a smaller area compared to that of the 1 km domain. The precipitation, 2 m temperature, 10 m wind speed, 2 m water mixing ratio, surface pressure, and long and shortwave radiation outputs from the

185 WRF 1 km simulations were bi-linearly re-gridded to the 100 m grid spacing in the high-resolution domain.

3.1 WRF standalone verification

The WRF model simulations were validated by using observations from 21 Automated Weather Stations (AWS) operated by the Norwegian Meteorological Institute (Fig. 3). These data were compared to the output of the 1 km simulations (Domain 2). The locations of the stations are given in Fig. 3 (top left panel), along with the location of Hardangerjøkulen. We note that

190 there exist additional stations in the south-west corner of the domain that were excluded in our evaluation because they were too close to the border of the domain. Figure 3 shows the total precipitation for the mass balance years 2015, 2016, 2017 and 2018 with observations given as colored circles. Here we define a mass balance year from October 1 in the previous year through September 30 of the current year. For example, the mass balance year 2015 ranges from October 1, 2014 to September 30, 2015. As can be seen in Fig. 3, the model captures the spatial precipitation distribution of the observed precipitation with

195 maximum precipitation near the coast and minimum to the lee of the mountains. The locations of some of these observations are in or near narrow fjords, such as the Ullensvang, Eidsfjord, Skulafossen, Kvamsøy and Øystese stations. These locations tend to underpredict precipitation by nearly 20% (see Fig. 4), which is a larger bias than stations further away from the fjords. Three of the stations (Finse, Midtstova and Geilo) are located at high-altitude exposed locations. At these stations there is a large under-catch of observed snow in the wintertime when the snow can blow past the precipitation gauges instead of falling

200 into the gauges (Rasmussen et al., 2012). The stronger the wind, the larger the under-catch. The data obtained from the Norwegian Meteorology Institute for these stations have not been corrected for any under-catch. Figure 5 show the effect of under-catch of snow at Finse, which is the station that is located closest to Hardangerjøkulen, about 4 km north-northeast of the glacier. In Fig. 5, the accumulated precipitation and temperature for the 2016 summer and winter season is shown at both Finse, Fet (a station about 25 km south west of Finse) and Evanger (a non-exposed inland station with little snow). Similar

205 results are seen for 2015, 2017 and 2018 (not shown). As can be seen, WRF compares well with observations at Evanger and Fet almost the entire period (Fig. 5a-5d). WRF precipitation also compares well with observations at Finse in the summer season (Fig. 5f), but has much more precipitation than the observations in the winter season (Fig. 5e) where wind speeds are often more than 5 m/s (Fig. 5i) and temperatures are below freezing. Furthermore, WRF does simulate the storm sequences

well as seen in Fig. 5g and 5h. Thus we attribute the low observed precipitation compared to WRF during the winter season at
210 Finse to the under-catch problem.

We conclude, as shown above, most of the non-exposed inland stations are relatively well simulated by the WRF-model and
the seasonal cycle of precipitation is captured. We note, however, one timeperiod where WRF is underpredicting the
precipitation relative to locations near Finse (Hardangerjøkulen). Several stations near Finse does not catch a precipitation
period in the middle of January 2017, which has an impact on Finse as well (this underprediction in WRF is difficult to directly
215 evaluate at Finse, but the two stations near Finse (Fet and Eidfjord) clearly have an underprediction at this time period (not
shown). We note that the observed storm sequences were captures in the simulation, wind direction was well simulated as well
as the wind speed, just not the precipitation amount. The effect of this precipitation time period will be discussed in relation to
the mass balance and streamflow results is Section 5.

Figure 6 shows a scatterplot of observed and simulated 2 m temperature at the Finse AWS. As can be seen, the modeled
220 temperature compares well with the observed, but with a small negative bias in the winter. At the very low observed
temperatures (< -15ºC), WRF often has a positive bias. This is likely due to WRF not capturing the strong inversions that
often occurs in the winter months (Mölders and Kramm, 2010; Hines et al., 2011). Figure 5e also shows this positive bias at
the very low temperatures. However, in general, WRF compares well with observations with a correlation coefficient near 0.9.

225 Figure 7 shows the simulated and observed 10 m wind speed and direction for the entire simulation period at Finse. Although
the wind direction is not an input variable in the land surface model in WRF-Hydro/Glacier, the wind direction can dictate
precipitation amount and type, thus wind direction is important for obtaining correct simulation of precipitation and subsequent
glacier mass balance as shown in Bhatt et al (2020)[1]. As can be seen, the simulated wind direction compares well with the
observed, but with a slightly higher frequency of wind from the west and from south-east compared to the observations.
230 Overall, the major simulated wind directions and speed are simulated quite well (see also Fig. 5 for wind speed).

4 Glacier observations

Hardangerjøkulen is a well observed glacier, with several decades of mass balance observations, and several field campaigns.
In the following, data from field observations, the ongoing mass balance observations and remote sensing are used to evaluate
the WRF-Hydro/Glacier system.

---

[1] * Note, text citing the Bhatt paper will be removed if that paper is not accepted by time (the Bhatt paper is listed as "to be submitted" in reference list)

4.1 Glacier mass balance

Glacier mass balance is the amount of surface mass a glacier gains or loses over a year (sum of accumulation and ablation). NVE has gathered winter, summer and annual (net) mass balance (winter + summer mass balance (where summer mass balance is negative)) observations over Rembesdalskåka since 1963 (nve.no/hydrologi/bre), where Rembesdalskåka is the west/south-west glacier outlet of Hardangerjøkulen (see Fig. 1). The observations are gathered at several locations on the glacier, from the lower to the upper parts (1066-1854 m a.s.l.) by using stakes (aluminum poles with graduated markings inserted into the glacier) and in spring by probing (using thin metal rods to measure snow depth) to the previous year's summer surface. Winter mass balance is found from the observed snow height (by stakes and rod soundings) and from snow density measurements at one location on the glacier. To determine summer balance, the observations are usually conducted at the end of the main melt season around the time period September - October, while the winter balance is usually determined at the end of the accumulation season May - June. Sometimes summer balance observations are conducted when new snow has accumulated. However, the summer surface can be found by evaluating the depth where the snow density representing the summer surface is found. To determine mass balance from the WRF-Hydro/Glacier simulations, we use the date with the smallest simulated glacier mass to determine the end of the summer and start of the winter season instead of using the actual date for when observations were gathered. Details about the annual mass balance observations are found in NVEs report series Glaciological investigations in Norway (Andreassen et al., 2016, 2017, 2019, Kjøllmoen et al., 2018).

4.2 Radar-derived snow thickness

Variations in snow accumulation were measured over Hardangerjøkulen in April 2017 and 2018, using ground-penetrating radar (GPR). In 2017, surveys were conducted with a MALA Geosciences GPR system; in 2018, this system was not available hence a Sensors & Software pulseEKKO PRO model was used instead. However, data from these two systems are directly compatible since both were acquired with antennas of 200 MHz center-frequency. The GPR systems were towed behind a snowmobile at ~15-20 km/h. With a 1 s sampling interval between successive GPR recordings, the spacing between datapoints is ~ 1 m. The position of the GPR was recorded with a GPS antenna mounted on the rear of the snowmobile, with positional accuracy of ~ 5 m. A total of 116 km and 27.4 km of measurements were acquired in 2017 and 2018, respectively, and both acquisitions featured numerous crossing-points such that the internal consistency of accumulation estimates could be ensured.

GPR systems record the travel-time of a radar pulse through the ground, therefore estimates of winter accumulation requires some measure of the GPR propagation velocity to covert time to depth. This was obtained using so-called common midpoint (CMP) data (e.g., Booth et al., 2011, 2013), in which GPR responses suggested an average velocity of 0.218 ± 0.001 m/ns for the upper ~ 2.8 m of the snowpack. With no other velocity control available, this value is applied to convert all GPR travel-time estimates to a snow depth.

265 The base of winter snow accumulation was taken to be the first prominent reflective horizon within the GPR record. This is straightforward in the Hardangerjøkulen ablation zone, typically at elevations ∼< 1600 m, where winter snow directly overlies the glacier surface, typically at a depth of 2-3 m. Here, the only significant reflection is from the glacier surface itself. Consequently, depth errors are expected to be less than ± 0.1 m. However, areas of firn accumulation have a more complex pattern of reflectivity and it is not always possible to guarantee accurate snow thicknesses, and errors may here be up to ± 1
270 m. However, given the crossing points in the GPR records, depth estimates are at least internally-consistent and errors are expected to vary systematically across the entire record.

4.3 MODIS snow albedo

The Crocus model computation of snow albedo depends on the physical properties of the snow grains, while the formulation used by Noah-MP model uses a time dependent empirical formulation. To evaluate the modeled snow albedo, we use the
275 NASA Moderate Resolution Imaging Spectrometer (MODIS) daily snow albedo product version 6 from Aqua (MYD10A1, Hall and Riggs, 2016a) and Terra (MOD10A1, Hall and Riggs, 2016b). These products are reported with 500 m grid spacing.

4.4 Streamflow

Discharge measurements were obtained at two rivers. One river (here named "Middalselvi") is fed by meltwater from the Midtdalsbreen (a glacier arm of Hardangerjøkulen) and the catchment is about 60% glacierized (see Fig. 2). The other river is
280 Finseelvi, where the catchment is 14.7% glacierized, and not much impacted by glacier melt. Two Hobo Water Level loggers were installed in each catchment in Fall of 2016 and we have data until November 2018.

5 Results

5.1 Glacier mass balance and snow height

Figure 8 shows the observed glacier mass balance, new accumulated snow thickness and density from NVE versus modeled
285 for the 2015-2018 mass balance years for Rembesdalskåka. The observed winter balance is taken from the locations shown in Figure 1 while the summer balance is found at 3 to 5 locations. The observed mass balance is plotted as averages in intervals of 50 - 100 m. For the summer balance all values between the 3 to 5 locations are interpolated. As can be seen, the modeled mass balance (winter, summer and net, Fig. 8a, d, g, and j) is generally comparable with the observations. The observed winter mass balance shows a small decrease at the top of the glacier, with a slight increase about 200 meters below the top (see left
290 panels). This is most likely due to redistribution of that is common at Finse and its surroundings, as strong winds occur often there. Since lateral redistribution of snow is not included in the Crocus and Noah-MP models, the modeled mass balance increases more linearly towards the top compared to the observations. The winter mass balance is about 29 % (20 %) underestimated in 2017 by Crocus (Noah-MP), which is likely due to the underprediction of winter precipitation at Finse and nearby stations in this year (discussed in section 3.1). For the three other years (2015, 2016 and 2018), the modeled winter

295   balance is within 9.3, 13.8 and 5.1 % (8.7, 14.7 and 2 %) of the observed winter mass balance for Crocus (Noah-MP)
respectively (see Fig. 9). However, note that Crocus matches better with the observations at lower levels below about 1500-
1600 m in 2017 and 2018 (see Fig. 8 left and middle panels). This does not show up in the total mass balance comparisons
since most of the mass is above 1600 m due to higher snow thickness and larger area (see Rembesdalskåka, Fig. 1). Another
point to add here is the improved simulation of winter mass balance of Rembesdalskåka compared to Engelhardt et al (2012).

300   They used gridded interpolated precipitaion data from seNorge (http://senorge.no) and obtained a mean negative bias of 28%
from 19 modeled winter mass balance years for Rembedalskåka, while we use high-resolution regional scale modeling to
obtain horizontally distributed precipitation.

For the summer and net mass balance we only consider Crocus since Noah-MP cannot melt more than the accumulated snow
amount from the model start (see Fig. 8, left panels). As the winter balance, the modeled summer mass balance is also in

305   general agreement with the observations with a bias of 6.67%, -1.5%, -7.4 % and 5.9 % in 2015, 2016, 2017 and 2018
respectively (Fig. 9). However, the modeled 2018 summer balance curve in Fig. 8j shows a different function of height
compared to the observations. This year the summer balance observations by NVE was taken late in the fall (November 22),
while the actual minimum was most likely in September based upon our model results. At this point, only the two top stakes
that are used to determine mass balance were left standing and both were located about 1750 m, while the other sakes had

310   melted out (Andreassen et al., 2019). Our model results compare favorably at the top altitudes where observations were
available. Below ~1750 m, there are no observations, and observed summer mass balance is instead estimated from observed
temperatures at nearby stations, and the relationship between temperature and melting for the period 2012-2017 (Andreassen
et al., 2020). Therefore, there is a possibility that our model results are closer in agreement to the actual melting than indicated
in Fig. 8j.

315   The modeled distribution of snow thickness and snow water equivalent (SWE) over Rembesdalskåka is comparable to
measurements by NVE (Fig. 10). The NVE data are the same as used in Fig. 8, while not averaged in elevation transects as in
Fig. 8. There is more heterogeneity in the observations, as would be expected since the models does not account for lateral
redistribution of snow. Despite this, Crocus does account for sublimation of snow drift, which results in more heterogeneity in
the spatial snow distribution over the glacier compared to Noah-MP. The relatively large underestimation of modeled SWE

320   (i.e. the winter balance) in 2017 is also seen in the snow thickness. This is also evident in Fig. 8, middle panel, which shows
the snow-depth as a function of altitude. The simulated snow-depth for 2015, 2016 and 2018 compare better with observations
at altitudes above 1600 m compared to the mass balance simulations (Fig. 8, left panel).

The observed densities for which the observed mass balance is based upon are 490, 481, 599 and 576 kg m^{-3} for the years
2015-2018 while the modeled Crocus snow densities, on average, are slightly lower (see Fig. 8, right panel). Snow densities

325   from Noah-MP are also slightly lower, but higher than the Crocus snow densities. In the first modeling year of 2015 Fig. 8c),
the snow density with Noah-MP is uniform over all elevations. However, as the simulations continued over several seasons

(Fig. (8f, 8i and 8l), the snow density increases with height for the following years. The reason for this increase is that Noah-MP only has three model layers. When new snow in the winter accumulates, some of this snow is merged with higher density multiyear snow from previous years in the accumulation zone of the glacier. It is therefore difficult to estimate the actual

330 modeled snow density of the new seasonal snow layer in the accumulation zone with Noah-MP in a multiyear simulation. The underestimation of density with Crocus is in agreement with Queno et al., (2016) who found that the bulk density in their study using Crocus also was underestimated and that Crocus tends to underestimate the snow compaction. On the other hand, since the density used to approximate the observed mass balance is taken from only one location, there are likely some uncertainties in the representability of this density over the entire glacier.

335 Ground penetrating radar observations were gathered in April 2017 and 2018. Note that this time period is not the same as when winter mass balance is determined with stake observations which occurred at the end or after the accumulation season (Fig. 10). Figure 11 shows both modeled and observed spatially distributed accumulated snow for the respective winter season, while Fig. 12 shows a 2-D histogram of the same data. Although these data show some scatter, and isolated observations significantly diverging from the model output (blue), the occurrence of such points is between 10-100 times lower than those

340 which plot close to the one-to-one comparison (red). As such, the majority of depths observed within the GPR dataset match the model outputs to within 1 m. Crocus has more variation in snow depth over the glacier compared to Noah-MP (see Fig. 12), but the modeled glacier in both snow models has less heterogeneity compared to the observations (Fig. 11). For 2017, we can see that there are areas over Rembesdalskåka where the model clearly underestimates the snow thickness, as can also be seen with the point observations from NVE in Fig. 10. However, at other locations on Rembesdalskåka the comparison is

345 favorable. Also, in the northern and western part of Hardangerjøkulen (the entire glacier complex) the model matches the observed snow thickness quite well. In the middle part of the glacier, Crocus estimates deeper snow-depth compared to Noah-MP and is closer in agreement with the observations both in 2017 and 2018.

5.2 Albedo

As discussed earlier, Crocus calculates albedo based upon the modeled snow properties, while Noah-MP albedo is dependent

350 on snow age alone. To compare modeled versus observed albedo, we use observations from MODIS-Terra and MODIS-Aqua daily snow cover and albedo products. Figure 13 shows the albedo near the top of the glacier, where the accumulated snow typically does not melt to bare ice during summer (see Fig. 1 for location). The grey dots represent albedo from MODIS-Terra and the black dots represents MODIS-Aqua albedo. Solid line is albedo from Crocus while dashed line is albedo from Noah-MP. The albedo is shown for the months May through August for each modeled year, thus the start of the melting season

355 is included. Figure 14 shows the same as Fig. 13 but closer to the north-north-west edge of the glacier (see Fig. 1 for location), where accumulated snow often completely melts during the summer season. As can be seen, the modeled albedo at both locations line up well with the observed albedo. The decrease in albedo at the end of the accumulation season, as the snow is aging, is well captured for both Noah-MP and Crocus. This is especially evident in 2015 in Fig. 14.

The rapid increase in albedo throughout the summer is due to snow events. The albedo determined with Crocus typically
360 decreases rapidly after an event since the albedo is based upon snow properties, the change of the snow properties over time
and the thickness of the snow layer. Noah-MP albedo, on the other hand, decreases slower after each snow event since it is
only dependent on the snow age. At the edge of the glacier (Fig. 14), the observations show a gradual decrease in albedo as
the snow starts to melt away to the bare ice (see for example July in 2016 and 2018 in Fig. 14), while the Crocus model has a
more abrupt decrease as the snow is completely melted away. The lowest value of albedo in Crocus over the ice is 0.35. The
365 Noah-MP does not have this decrease in albedo as the land surface category over glacier grid points is assumed to be that of
old snow with minimum albedo of 0.675. Therefore, since snow in the three-layer snow model is allowed to have lower albedo
than 0.675, when the bare land surface category (glacier) is revealed, the albedo actually increases (see 2018 in Fig. 14). The
correlation coefficients between modeled and observed albedo is given in Table 1. Overall, the Crocus albedo compares much
better with the observations than the Noah-MP albedo in the summertime when the snow melts and the ice becomes apparent
370 due to the assumption of glacier land surface category in Noah-MP.

5.3 Discharge

Figure 2 includes the catchment areas of the Middalselvi (which is fed by Midtdalsbreen) and Finseelvi, locations where
discharge measurements were gathered in 2017 and 2018. Figure 15 shows the modeled and observed discharge in Middalselvi
for summer 2017 and 2018. Also shown is the daily precipitation at Finse station. The modeled precipitation at Finse AWS
375 station compares well with the observed, except for one precipitation event in late July 2017, where the model predicts too
much precipitation at the Finse station. During the precipitation events, both the Crocus and Noah-MP simulations and
observations show increases in discharge but with some variability in strength. Interestingly, during the large dry events in the
end of June and through most of July of 2018, the modeled and observed discharge is very similar.

In regards to the observed peak flow at the beginning of melt season in May, the model does not predict such a peak flow.
380 These peaks mark the onset of the hydrologic season in the rivers. They occurred almost at the same time in the two catchments
in two consecutive years under similar preconditions. Photographs taken on site prior the event indicate that water was flowing
over the snow pack and was carving down to the river bed during the event. Probably some part of the peak is due to a pulsed
meltwater flux and/or the associated pressure build up to that time which is subsequently released. Therefore, when evaluating
the accumulated discharge, we start the accumulated period directly after the large spike in the observations. The accumulated
385 discharge for 2017 shows that the observations are slightly higher than the discharge simulated with WRF-Hydro/Glacier (with
Crocus). They still follow closely, but WRF-Hydro/Glacier flattens out in the fall earlier compared to observations. This is
likely due to lack of groundwater in these specific WRF-Hydro/Glacier simulations. The WRF-Hydro simulations with only
Noah-MP is consistently much lower compared to both observations and WRF-Hydro/Glacier at Middalselvi. For 2018,
simulations with both Noah-MP over the glacier and Crocus over the glacier follow the observations reasonably well, however
390 they both overpredict the discharge in the end of May and early June. Around July 30, the Crocus simulations increase slightly

more than the observations while the Noah-MP simulations reduce discharge considerably at the end of August. The Crocus simulations still have discharge comparable with the observations until September. As shown in Fig. 8j, Crocus has a larger negative summer mass balance compared to the observations which, for which the large discharge in early June in both Noah-MP and Crocus is likely connected to. Thus, even though Noah-MP compares well with observations at the end of the melt season in 2018, this is most likely due to too much melt in the beginning of the melt season and not the skill of the Noah-MP simulations.

One of the reasons for the lower discharge in Middalselvi with the Noah-MP compared to Crocus is likely the lack of glacier runoff once the seasonal snowpack has melted. The Middalselvi is about 60% glacierized, while Finseelvi is only 14.7% glacierized. As can be seen in the discharge data for Finseelvi (Fig. 16), the Noah-MP compares better with the observations in the entire melt season than it does for Middalselvi (especially in 2017, in 2018 the discharge is too high in end of May and beginning of June as discussed above). Crocus is not shown in Fig. 16 since the Crocus simulation only feeds rivers downstream of Hardangerjøkulen and the WRF-Hydro/Glacier system uses the Noah-MP snow model in the Finseelvi catchment area.

We hypothesize that a second reason for the lower discharge with Noah-MP compared to Crocus is likely the albedo treatment. In 2017, there are many small snow accumulation events. This causes the Noah-MP albedo to rarely go below 0.7 at the top of the glacier (Fig. 13). However, both observations and Crocus simulations have albedo closer to 0.6. At the edge of the glacier (Fig. 14), the times where Crocus is close to 0.6 is longer, and in August, the albedo for both Crocus and the observations are around or below 0.4. For 2018, the albedo of Noah-MP and Crocus both compares well with the observations at the top of the glacier, due to the prolonged dry periods (no new snow events that lead to overestimation of albedo in Noah-MP). During this dry time period, the discharge from Noah-MP and Crocus are comparable. At the edge of the glacier, Noah-MP overestimate the albedo from end of July. This is when all accumulated snow is melted and the surface is bare ice. The Noah-MP albedo increases to 0.67 (that of old snow), while Crocus and observations indicate that the albedo should be that of ice. This is also the time period where streamflow from Noah-MP significantly diverge from Crocus. As an illustration we re-ran Crocus for the 2018 season and substituted ice albedo with snow albedo. Figure 17 shows the accumulated streamflow with the sensitivity study (red curve). It is clear that the streamflow is reduced compared to the original simulation from the end of July at the time period where surface albedo at the edge of the glacier is reduced to that of ice. Bonekamp et al. (2019) found that the recharge of snow albedo from summer snow events in their simulations (WRF with Noah-MP) over glaciers in the Shimsal catchment in Karakoram had large impact on the summer mass balance. We remind that even though the final accumulated streamflow using snow albedo instead of ice albedo seem to be more in line with observations, this assumption does not actually improve the simulation as it reduces the streamflow for the wrong reason.

Finally, it should also be noted that WRF-Hydro and WRF-Hydro/Glacier has not been calibrated due to lack of non-restricted streamflow measurements in the area. And while we have calibrated some parameters in Crocus, we used all default values in Noah-MP. These are all factors that can contribute to biases and uncertainties in the simulations.

6 Conclusion

425 The detailed physically-based snow model Crocus was implemented into the WRF-Hydro system to act as a glacier model. This model supports a large number of snow layers with dynamic density, thickness and snow properties. Furthermore, the albedo is prognostically calculated based on the physical properties of the snow. The implementation of Crocus allows for a direct estimation of glacier surface winter, summer and net balance. The snow accumulation is already represented reasonably well within the WRF model when using Noah-MP land surface model. However, the results of comparative studies performed

430 here show that the Crocus snow model improves the simulation of melting ice by allowing for snow to melt to bare ice, and using the albedo of ice for further melting, instead of an assumed albedo over glacier land surface category. This is critical for representation of glacier wastage during the summer season. Furthermore, the integration of Crocus with WRF-Hydro allows for the discharge to be directly affected by the melting ice. Major conclusion of the evaluation of implementation of the WRF-Hydro/Glacier system and the input forcing are summarized as follows:

435 - WRF produces meteorological forcing data comparable with the observations. For example, the temperature and wind speed at Finse are in excellent agreement. The 1-km grid spacing simulation results are used for input to the WRF-Hydro/Glacier system to evaluate glacier surface mass balance and subsequent streamflow.

- Observed solid precipitation on Finse is affected by under-catch due to strong winds. Using observed precipitation from this location without correcting for this under-catch will result in an underestimation of winter surface mass

440 balance. However, the high-resolution model simulations with WRF at 1 km shows an excellent ability in producing winter precipitation.

- The simulations with Crocus are doing a reasonable job in reproducing winter, summer and annual surface mass balance with bias of less than 11% in summer and about 15 % in winter (excluding 2017 which have a bias in forcing data). Noah-MP is doing slightly better than Crocus in simulating winter mass balance, but cannot be used for directly

445 evaluating the summer mass balance since Noah-MP can only melt accumulated snow from simulation start and there is a lack of preexisting ice in the initialization of the simulation.

- Snow depth is reproduced well, both compared with the GPR observations and observations from NVE (except 2017 compared with the NVE observations). However, the mean snow density with Crocus and Noah-MP is 5-20%

underestimated compared to NVE observations, suggesting that some of the inconsistency of snow depth (little bias) and mass balance (some bias) comparison is due to the bias in modeled snow density.

- By applying Crocus over a glacier, the surface albedo is better represented in the ablation region where ice (with lower albedo compared to snow albedo) becomes present. This allows for better representation of melting and subsequent discharge in a glacier dominated catchment with WRF-Hydro/Glacier.

In conclusion, both the more physically based snow model Crocus, and Noah-MP are simulating the winter mass balance and snow thickness well. The WRF-Hydro discharge simulations in the minimally glacierized, lower-elevation catchment (Finseelvi) are also reasonable with the Noah-MP model (keeping in mind that neither WRF-Hydro nor WRF-Hydro/Glacier has been calibrated for the simulated region). Despite this, WRF-Hydro/Glacier shows more realistic performance in the glacierized catchment due to the fact that it allows modeling of negative net mass balance and uses ice surface albedo where all accumulated snow is melted, both elements which Noah-MP currently does not include. Finally, we note that we have not currently included lateral movements of the glacier or any treatment of blowing snow in WRF-Hydro/Glacier. The impacts of including these additional physical processes may afford additional improvements in annual snowpack and snowmelt representation, particularly with respect to their spatial distribution. More development and testing of WRF-Hydro/Glacier are certainly required and are currently underway. In particular the system should be applied and assessed over other glaciated regions of the world. It is a tool that can contribute to better understanding of future hydroclimate; especially in light of the continued widespread glacier retreat and decline in mass balance, which has profound implications for future water resources in many parts of the world.

Achnowledgement

This work has been funded through the Research Council of Norway (RCN) through EvoGlac (grant no. 255049). The hydrologic fieldwork is funded by the Strategic Research Initiative 'Land Atmosphere Interaction in Cold Environments' (LATICE) of the University of Oslo. Radar fieldwork was part-funded by the European Union's Horizon 2020 INTERACT project, under grant agreement No 730938 'Snow Accumulation Patterns on Hardangerjøkulen Ice Cap (SNAP)', NERC SPHERES DTP grant NE/ L00257 and NERC Industrial CASE Studentship NE/P009492/1. Field surveys were supported by Emma Pearce and Siobhan Killingbeck (University of Leeds) and the logistics expertise of Kjell Magne Tangen (Tajo AS). Jostein Bakke (University of Bergen) supplied the GPR system for the 2017 survey. Atle Nesje received in-kind funding from Department of Earth Science at UiB. Kjetil Melvold received in-king funding from NVE. The National Center for Atmospheric Research is sponsored by the U.S. National Science Foundation (NSF).

References

480 Andreassen, L.M., and Winsvold, S.H. (eds.).: Inventory of Norwegian glaciers. NVE Report 38, Norges Vassdrags- og energidirektorat, 236 pp, 2012.

Andreassen, L. M., Elvehøy, H., Jackson, M., Kjøllmoen, B and Giesen, R. H.: Glaciological investigations in Norway in 2011-2015, edited by: Kjøllmoen, B., NVE Report 88/2016, Norwegian Water Resources and Energy Directorate, 2016.

Andreassen, L. M., Elvehøy, H., Jackson, M., Melvold, K., and Kjøllmoen, B.: Glaciological investigations in Norway in
485 2016, edited by: Kjøllmoen, B., NVE Report 76/2017, Norwegian Water Re- sources and Energy Directorate, 2017.

Andreassen, L. M., Elvehøy, H. and Jackson, M.: Glaciological investigations in Norway in 2018, edited by: Kjøllmoen, B., NVE Report 46/2019, Norwegian Water Reources and Energy Directorate, 2019.

Arnault, J., Rummler, T., Baur, F., Lerch, S., Wagner, S., Fersch, B., Zhang, Z., Kerandi, N., Keil, C., and Kunstmann, H: Precipitation sensitivity to the Uncertainty of Terrestrial Water Flow in WRF-Hydro: An Ensemble Analysis for Central
490 Europe, J. Hydrometeor., 19, 1007–1025, doi:10.1175/jhm-d-17-0042.1, https://doi.org/10.1175/JHM-D-17-0042.1, 2018.

Bhatt, B.C., Sorteberg, A., Eidhammer, T., and Nesje, A.: High-resolution atmosphere/surface modelling of the Hardangerjøkulen Glacier mass balance and its dependence on meteorological conditions. To be submitted (*Note: reference to this paper in the text will be removed if paper is not accepted in time*), 2020.

Bonekamp, P. N. J., de Kok, R. J., Collier, E., Immerzeel, W. W.: Contrasting meteorological drivers of the glacier mass
495 balance between the Karakoram and central Himalaya, Frontiers in Earth Science, Volume 7, id.107, https://doi.org/10.3389/feart.2019.00107, 2019.

Bolch, T., Kulkarni, A., Kääb, A., Huggel, C., Paul, F., Cogley, J.G., Frey, H., Kargel, J.S., Fujita, K., Scheel, M., Bajracharya, S., Stoffel, M.: The state and fate of Himalayan glaciers. Science 336, 310–314, DOI: 10.1126/science.1215828, 2012.

Booth, A.D., Clark, R.A. and Murray, T.: Influences on the resolution of GPR velocity analyses and a Monte Carlo simulation
500 for establishing velocity precision. Near Surface Geophysics, 9, 399-411. doi: 10.3189/2013AoG64A044, 2011.

Booth, A.D., Mercer, A., Clark. R. A., Murray, T., Jansson, P. and Axtell, C.: A comparison of seismic and radar methods to establish the thickness and density of snow cover. Annals of Glaciology. 54(64), 73-82. doi:10.3997/1873-0604.2011019, 2013.

Brun, E., Martin, E., Simon, V., Gendre, C., and Col´eou, C.: An energy and mass model of snow cover suitable for operational
505 avalanche forecasting, J. Glaciol., 35, 333–342, DOI: https://doi.org/10.3189/S0022143000009254, 1989.

Brun, E., David, P., Sudul, M., and Brunot, G.: A numerical model to simulate snow-cover stratigraphy for operational avalanche forecasting, J. Glaciol., 38, 13–22, DOI: https://doi.org/10.3189/S0022143000009552, 1992.

Brun, E., Martin, E., and Spiridonov, V.: Coupling a multi-layered snow model with a GCM, Ann. Glaciol., 25, 66–72, DOI: https://doi.org/10.3189/S0260305500013811, 1997.

510 Collier, E., Mölg, T.,Maussion, F., Scherer, D.,Mayer, C., and Bush, A. B. G.: High-resolution interactive modelling of the mountain glacier–atmosphere interface: an application over the Karakoram. Cryosphere 7, 779–795. doi: 10.5194/tc-7-779-2013, 2013.

Engelhardt, M., Schuler, T. V., Andreassen L. M.: Evaluation of gridded precipitation for Norway using glacier mass-balance measurements. Geografiska Annaler: SeriesA, Physical Geography94: 501–509. DOI:10.1111/j.1468-0459.2012.00473.x,
515 2012.

Fersch, B., Senatore, A., Adler, B., Arnault, J., Mauder, M., Schneider, K., Völksch, I., and Kunstmann, H.: High-resolution fully-coupled atmospheric–hydrological modeling: a cross-compartment regional water and energy cycle evaluation, Hydrol. Earth Syst. Sci. Discuss., https://doi.org/10.5194/hess-2019-478, in review, 2019.

Gerbaux, M. et al.. Surface mass balance of glacier in the French Alps: Distributed modeling sensitivity to climate change. J.
520 of Glaciol. 175(51), 561-572(12), DOI: https://doi.org/10.3189/172756505781829133, 2005.

Gochis, D.J. et al.: The WRF-Hydro Model Technical Description and User's Guide, Version 3.0. NCAR Technical Document. 120 p. Available at: http://www.ral.ucar.edu/projects/wrf_hydro/. WRF-Hydro 30 User Guide, 120 p, 2015.

Hall, D. K. and Riggs, G. A.: *MODIS/Aqua Snow Cover Daily L3 Global 0.05Deg CMG, Version 6*. Boulder, Colorado USA. NASA   National   Snow   and   Ice   Data   Center   Distributed   Active   Archive   Center,
525 doi: https://doi.org/10.5067/MODIS/MYD10C1.006, 2016

Hall, D. K. and Riggs, G. A.: *MODIS/Terra Snow Cover Daily L3 Global 500m SIN Grid, Version 6*. Boulder, Colorado USA. NASA   National   Snow   and   Ice   Data   Center   Distributed   Active   Archive   Center, doi: https://doi.org/10.5067/MODIS/MOD10A1.006, 2016

Hines, K. M., Bromwich, D. H., Bai, L.-S., Barlage, M., and Slater, A. G.: Development and testing of Polar WRF. Part III:
530 Arctic land, J. Climate, 24, 26–48, https://doi.org/10.1175/2010JCLI3460.1, 2011.

Hong, S-Y, Noh, Y., Dudhia, J.: A new vertical diffusion package with an explicit treatment of entrainment processes. Mon Wea Rev 134:2318–2341, https://doi.org/10.1175/MWR3199.1m, 2006.

Iacono, M. J., Jennifer, S. D., Eli, J. M., Mark, W. S., Shepard, A. C., and William, D. C.: Radiative forcing by long-lived greenhouse gases: calculations with the AER radiative transfer models. J. Geophys. Res. Atmos. 113:D13103.
535 doi:10.1029/2008JD009944, 2008.

Immerzeel, W. W., Beek, L. P. H. V., and Bierkens, M. F. P.: Climate change will affect the Asian water towers. Science 328, 1382–1385. doi: 10.1126/science. 1183188, 2010.

Immerzeel, W.; Pellicciotti, F.; Bierkens, M.: Rising river flows throughout the twenty-first century in two Himalayan glacierized watersheds. Nat. Geosci, 6, 742, https://doi.org/10.1038/ngeo1896, 2013.

540   Kaser, G., Großhauser, M., and Marzeion, B.: Contribution potential of glaciers to water availability in different climate regimes. Proc. Natl. Acad. Sci. U.S.A. 107, 20223–20227. doi: 10.1073/pnas.1008162107, 2010.

Kjøllmoen, B., Andreassen, L. M., Elvehøy, H. and Jackson, M.: Glaciological investigations in Norway in 2017, edited by: Kjøllmoen, B., NVE Report 82/2018, Norwegian Water Resources and Energy Directorate, 2018.

Kotlarski, S., Paul, F., and Jacob, D.: Forcing a distributed glacier mass balance model with the regional climate model REMO.
545   Part I: climate model evaluation, J. Climate, 23, 1589–1606, https://doi.org/10.1175/2009JCLI2711.1, 2010.

Laghari, J. R.: Climate change: Melting glaciers bring energy uncertainty. Nature. 503(7477): 464-464, doi:10.1038/502617a, 2013.

Li, L., Gochis, D.J., Sobolowski, S., Mesquita, M.D.S.: Evaluating the present annual water budget of a Himalayan headwater river basin using a high-resolution atmosphere-hydrology model. J. Geophys. Res. 122, 4786–4807,
550   https://doi.org/10.1002/2016JD026279, 2017.

Lundquist, J., Hughes, M., Gutmann, E., and Kapnick, S.: Our skill in modeling mountain rain and snow is bypassing the skill of our observational networks. *Bull. Am. Meteorol. Soc.* doi: 10.1175/BAMS-D-19-0001.1, 2020.

Machguth, H., Paul, F., Kotlarski, S. and Hoelzle, M.: Calculating distributed glacier mass balance for the Swiss Alps from regional climate model output: a methodical description and interpret- ation of the results. J. Geophys. Res. Atmos., 114(19),
555   1–19 (doi:10.1029/2009JDO11775), 2009.

Melvold, K., Laumann, T. and Nesje, A.: Kupert landskap under Hardangerjøkulen [Online]. Norge: GEO. http://www.geoforskning.no/reportasjene/38-kupert-landskap-under-hardangerjokulen, 2011.

Mölders, N., Kramm, G.: A case study on wintertime inversions in Interior Alaska with WRF. Atmos Res 95(2–3):314–332, https://doi.org/10.1016/j.atmosres.2009.06.002, 2010.

560   Mölg, T. and Kaser, G.: A new approach to resolving climate– cryosphere relations: downscaling climate dynamics to glacier-scale mass and energy balance without statistical scale linking, J. Geophys. Res., 116, D16101, DOI: 10.1029/2011JD015669, 2011.

Niu, G. Y., Yang, Z. L., Mitchell, K. E., Chen, F., Ek, M. B., Barlage, M., et al.: The community Noah land surface model with multiparameterization options (Noah-MP): 1. Model description and evaluation with local-scale measurements. J.
565   Geophys. Res. Atmos. 116, 1–19. doi: 10.1029/2010JD015139, 2011.

Proksch, M., Rutter, N., Fierz, C., and Schneebeli, M.: Intercomparison of snow density measurements: bias, precision, and vertical resolution, The Cryosphere, 10, 371–384, doi:10.5194/tc- 10-371-2016, 2016.

Quéno, L., Vionnet, V., Dombrowski-Etchevers, I., Lafaysse, M., Dumont, M., and Karbou, F.: Snowpack modelling in the Pyrenees driven by kilometric-resolution meteorological forecasts. Cryosphere 10, 1571–1589. doi: 10.5194/tc-10-1571-2016, 2016.

Rasmussen, R., Baker, B., Kochendorfer, J., Meyers, T., Landolt, S., Fischer, A. P., et al.: How well are we measuring snow: the NOAA/FAA/NCAR winter precipitation test bed. Bull. Am. Met. Soc. 93, 811–829. doi: 10.1175/BAMS-D-11-00052.1, 2012.

Revuelto, J., Vionnet, V., López-Moreno, J.-I., Lafaysse, M., and Morin, S.: Combining snowpack modeling and terrestrial laser scanner observations improves the simulation of small scale snow dynamics. J. Hydrol. 533, 291–307. doi: 10.1016/j.jhydrol.2015.12.015, 2016.

Rummler, T., Arnault, J., Gochis, D., and Kunstmann, H.: Role of Lateral Terrestrial Water Flow on the Regional Water Cycle in a ComplexTerrain Region: Investigation With a Fully Coupled Model System, J. Geophys. Res. Atmos., 0, doi:10.1029/2018jd029004, 2019.

Senatore, A., Mendicino, G., Gochis, D. J., Yu, W., Yates, D. N. and Kunstmann, H.: Fully coupled atmosphere-hydrology simulations for the central Mediterranean: Impact of enhanced hydrological parameterization for short and long time scales, J. Adv. Model. Earth Syst., 7, 1693–1715, doi:10.1002/2015MS000510, 2015.

Skamarock, W. C., Klemp, J. B., Dudhi, J., Gill, D. O., Barker, D. M., Duda, M. G., et al.: A Description of the Advanced Research WRF Version 3. Technical Report 113. NCAR, Tech. Note, Mesoscale and Microscale Meteorology Division. National Center for Atmospheric Research, Boulder, Colorado, USA, 2008.

Sorg, A. et al.: Climate change impacts on glaciers and runoff in Tien Shan (Central Asia). Nature Climate Change 2(10): 725-731, https://doi.org/10.1038/nclimate1592, 2012.

Thompson, G.; Eidhammer, T.: A study of aerosol impacts on clouds and precipitation development in a large winter cyclone. J. Atmos. Sci. 71, 3636–3658, https://doi.org/10.1175/JAS-D-13-0305.1, 2014.

van Pelt, W. J. J., Oerlemans, J., Reijmer, C. H., Pohjola, V. A., Pettersson, R., and van Angelen, J. H.: Simulating melt, runoff and refreezing on Nordenskiöldbreen, Svalbard, using a coupled snow and energy balance model, The Cryosphere, 6, 641–659, https://doi.org/10.5194/tc-6-641-2012, 2012.

Vionnet, V., Brun, E., Morin, S., Boone, A., Faroux, S., Le Moigne, P., et al.: The detailed snowpack scheme Crocus and its implementation in SURFEX v7.2. Geosci. Model. Dev. 5, 773–791. doi: 10.5194/gmd-5-773-2012, 2012.

Vionnet, V., Six, D., Auger, L., Dumont, M., Lafaysse, M., Quéno, L., Réveillet, M., Dombrowski-Etchevers, I., Thibert, E. and Vincent, C.: Sub-kilometer Precipitation Datasets for Snowpack and Glacier Modeling in Alpine Terrain. Front. Earth Sci. 7:182. doi: 10.3389/feart.2019.00182, 2019.

Willemet, J. M., 2008: The snow cover model: CROCUS user's guide (Version 2.4), 2008.

Yucel, I., Onen, A., Yilmaz, K. K., and Gochis, D. J.: Calibration and evaluation of a flood forecasting system: Util- ity of
600   numerical weather prediction model, data assimi- lation and satellite-based rainfall, J. Hydrol., 523, 49–66,
https://doi.org/10.1016/j.jhydrol.2015.01.042, 2015.

605

610

615

620

Tables

Table 1: Correlation coefficient between simulated and observed albedo. Values outside parenthesis are albedo from Modis Aqua while values inside parenthesis are albedo from Modis Terra.

630

Year -> Model	2015	2016	2017	2018
Crocus (top)	0.74 (**0.88**)	**0.54** (0.67)	0.69 (**0.64**)	**0.36** (0.42)
Noah-MP (top)	0.59 (0.77)	0.01 (0.12)	-0.14 (-0.27)	0.32 (0.51)
Crocus (edge)	**0.89** (0.89)	0.81 (**0.83**)	**0.89** (0.80)	**0.82** (0.85)
Noah-MP (edge)	0.71 (0.90)	-0.33 (-0.21)	-0.06 (-0.21)	0.15 (0.36)

635

640

Figures
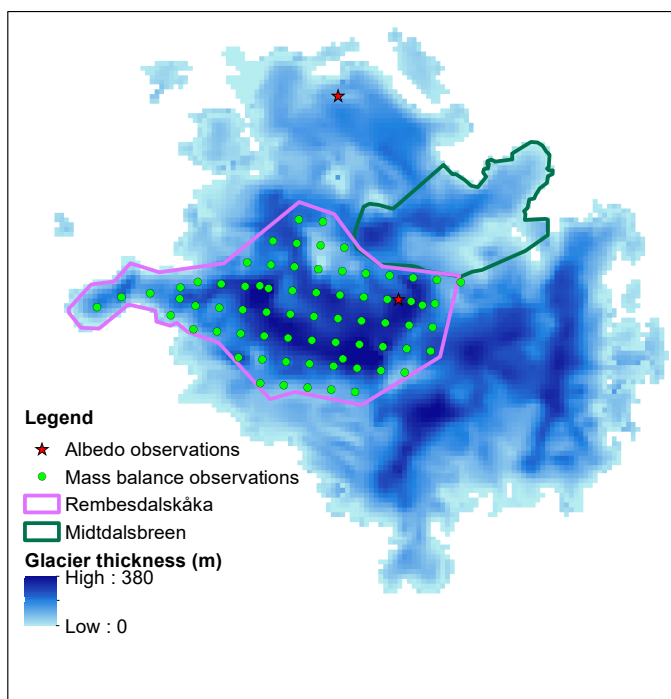
645

Figure 1: Glacier thickness and present extent for Hardangerjøkulen. The outlet glaciers Rembesdalskåka, Midtdalsbreen are also indicated. The green dots indicate locations where stake observations for winter balance were obtained. Stars shows location of
650 **albedo comparison with model against observations.**
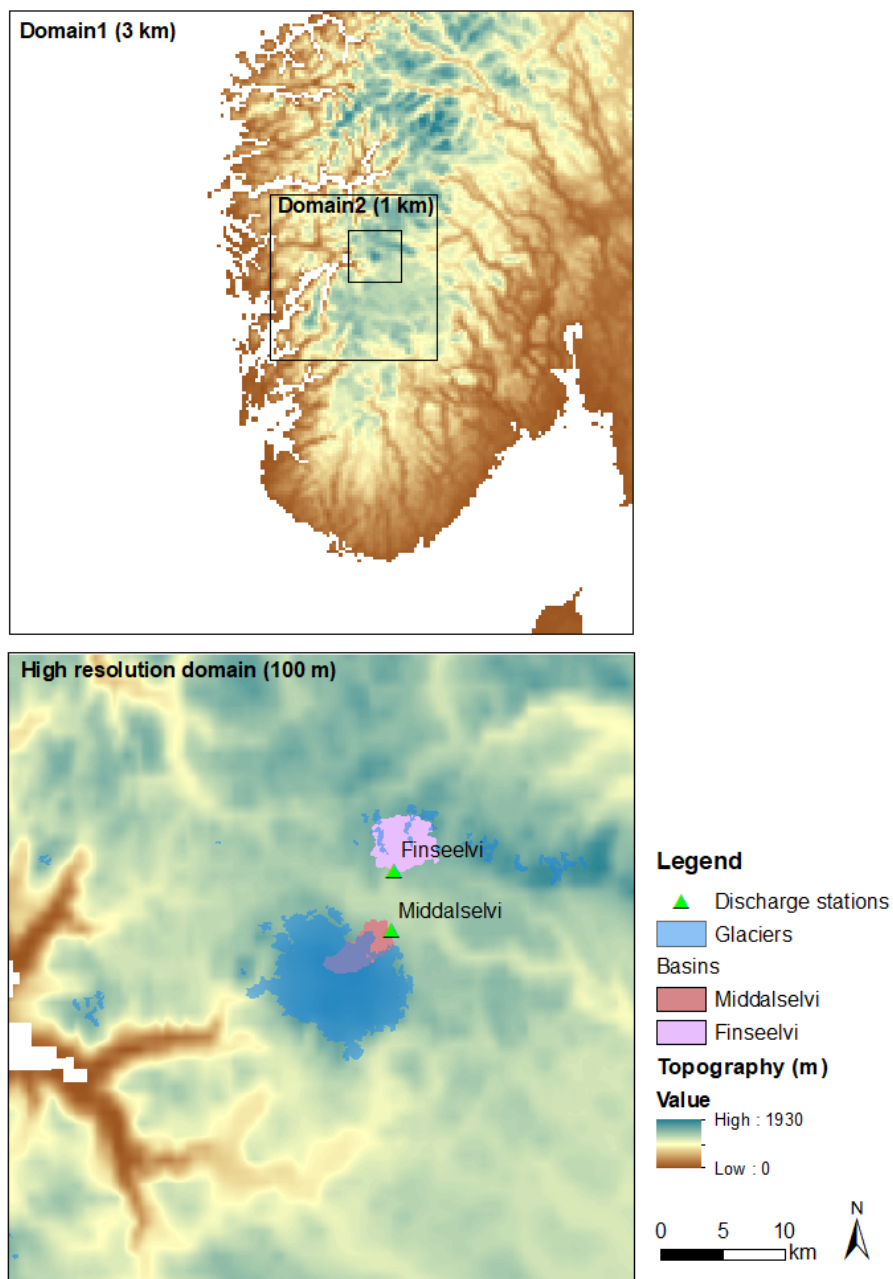
Figure 2: Model domains. The top figure shows the WRF domains with 3 km and 1 km grid spacing. The bottom figure shows the domain of the high resolution (100 m grid spacing) used with WRF-Hydro/Glacier. Furthermore, the outline of Hardangerjøkulen and the river basins of the two rivers with discharge observations are included as well.

655
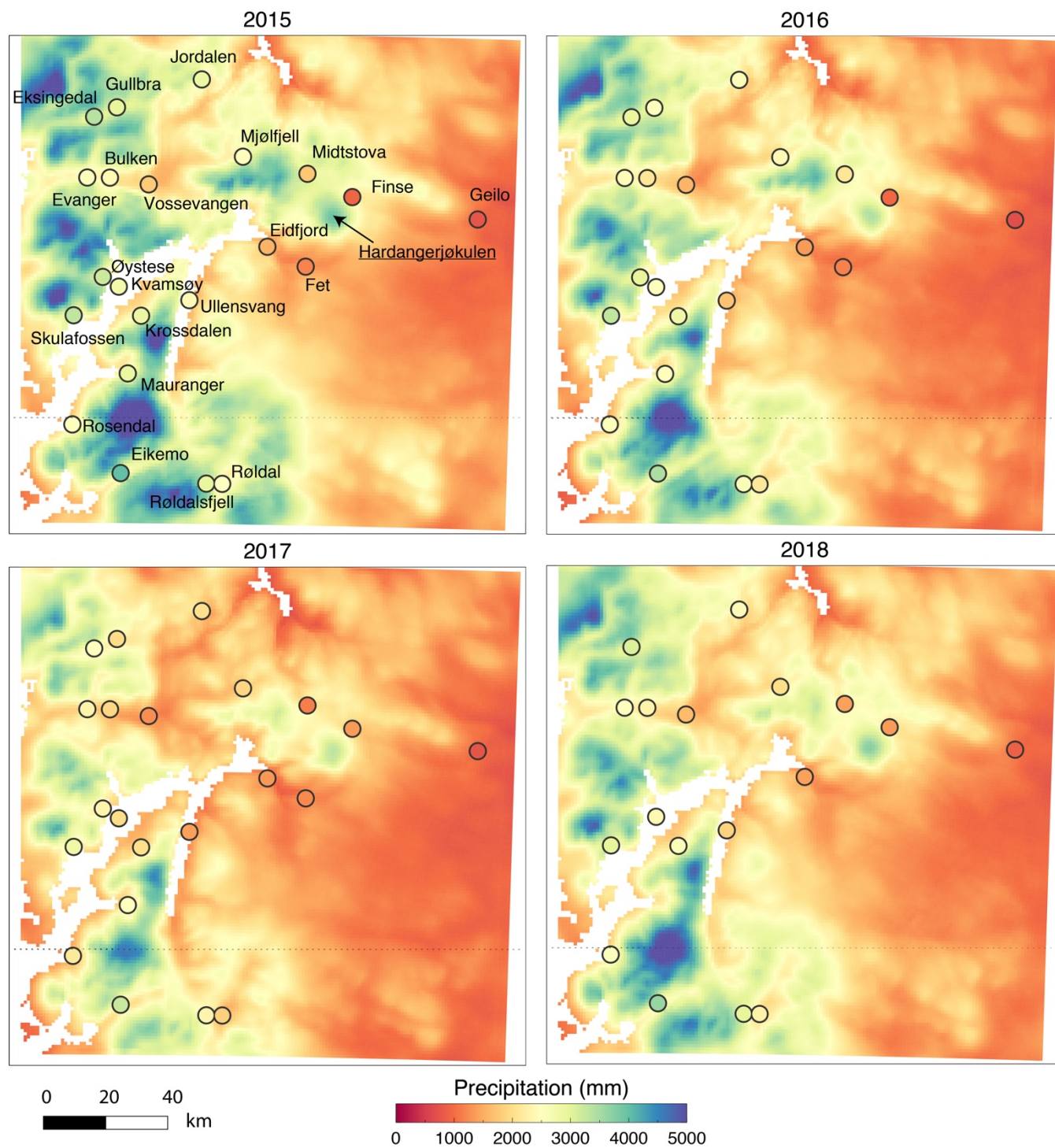
Figure 3: Simulated and observed precipitation (October – September) for mass balance years 2015-2018. Circles represent observations from AWS. The location of Hardangerjøkulen is also indicated.

660
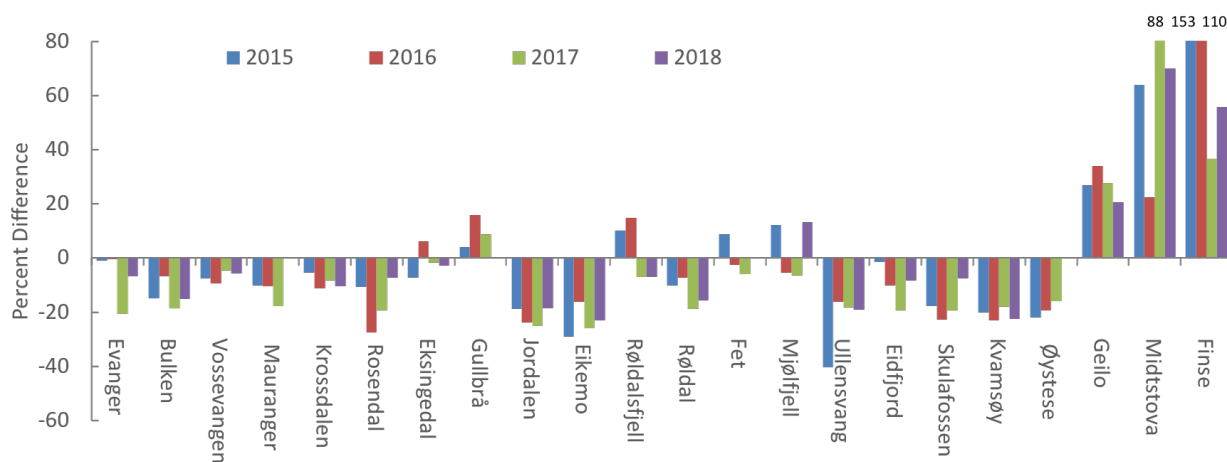
Figure 4: Percent difference in simulated and observed precipitation at all stations for mass balance years 2015-2018. Some values above Midtstova and Finse are above the axis limit and are therefore indicated with labels.

665
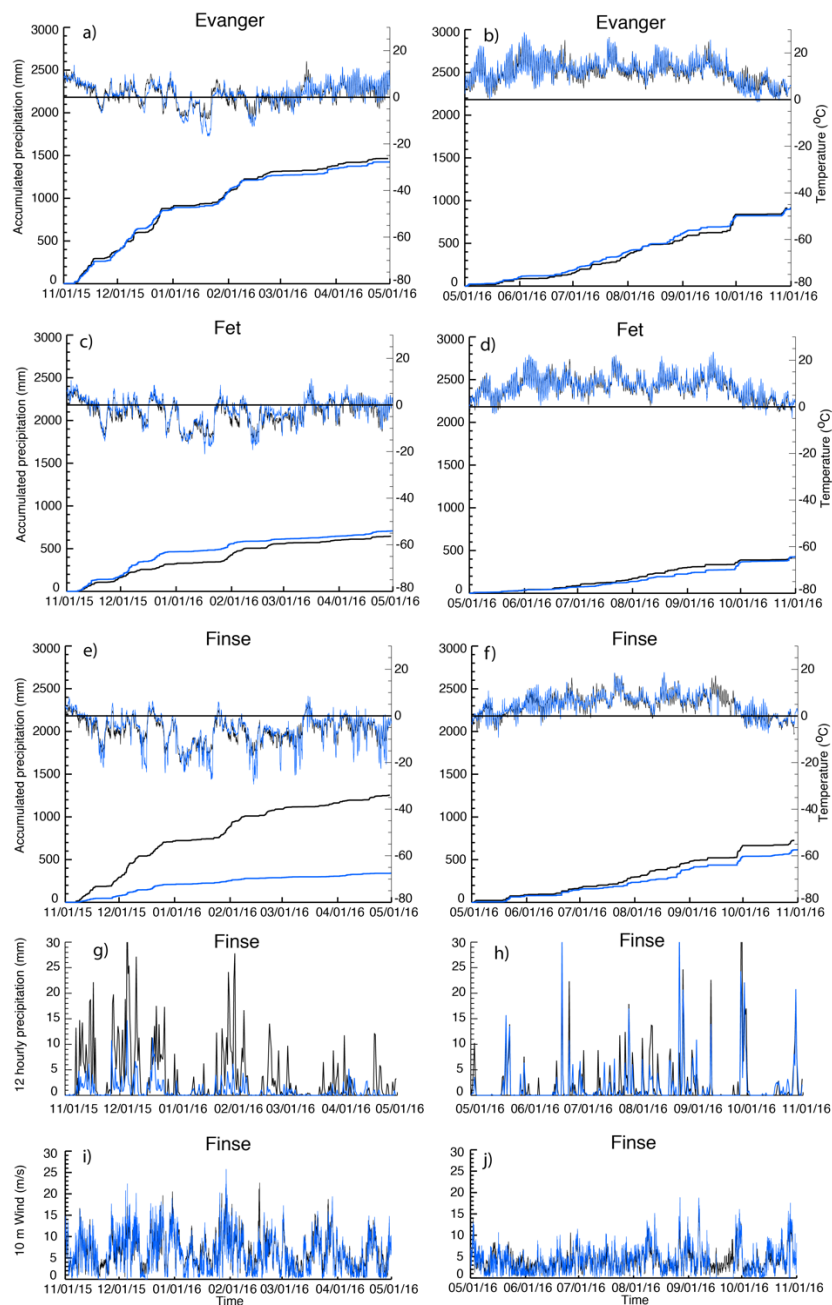
Figure 5: Observed (blue) and modeled (black) accumulated precipitation and temperature at Evanger (a, b), Fet (c, d) and Finse (e, f) stations for the 2016 winter season (left panel) and 2016 summer season (right panel). g) and h) shows time series of precipitation. The bottom panel (i, j) shows the 10 m wind speed at Finse.
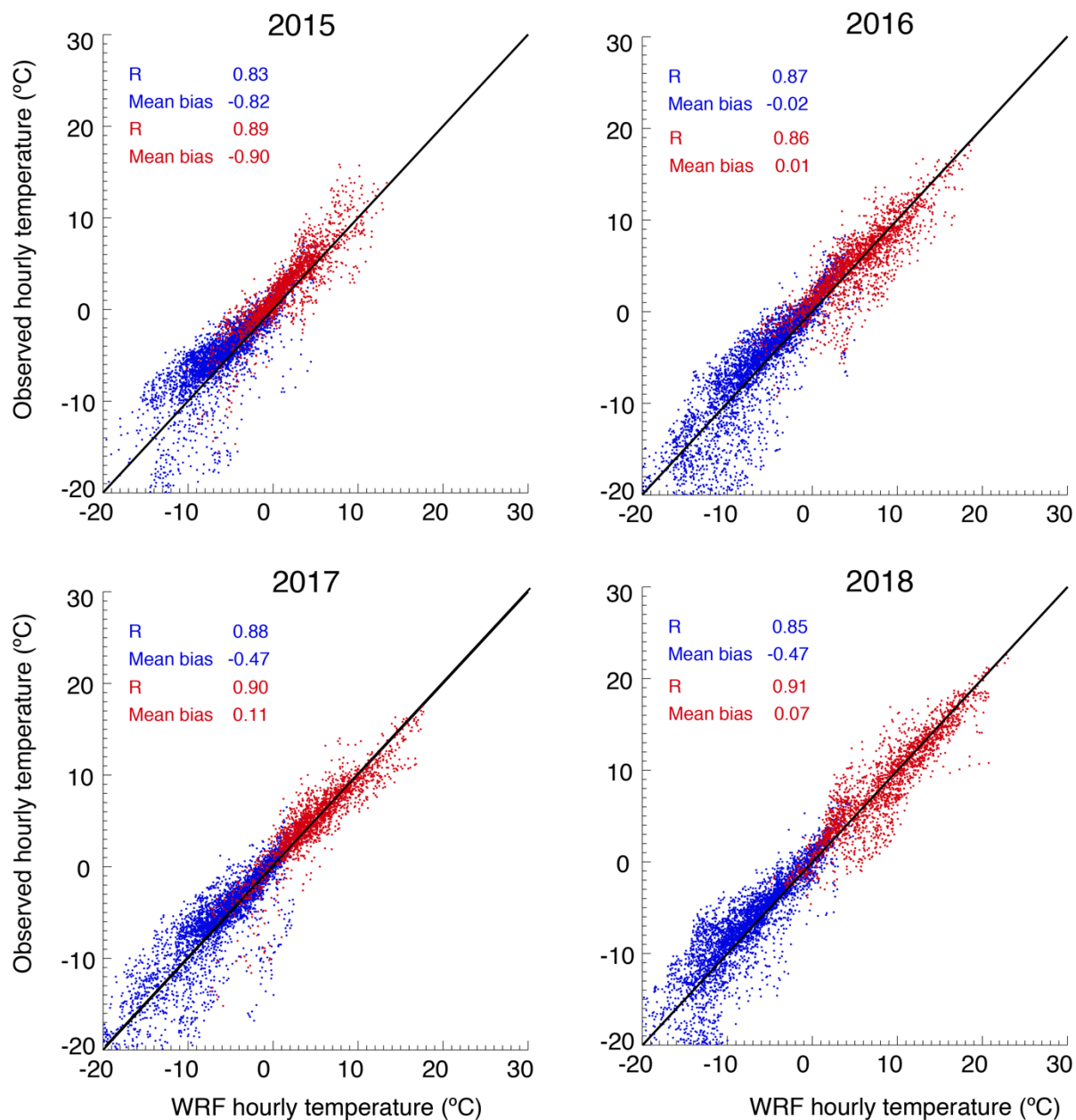
Figure 6: Scatterplot of observed and simulated temperature for mass balance years 2015-2018 at Finse station. Blue colors represent
675 **the winter season and red colors represent summer season.**

680
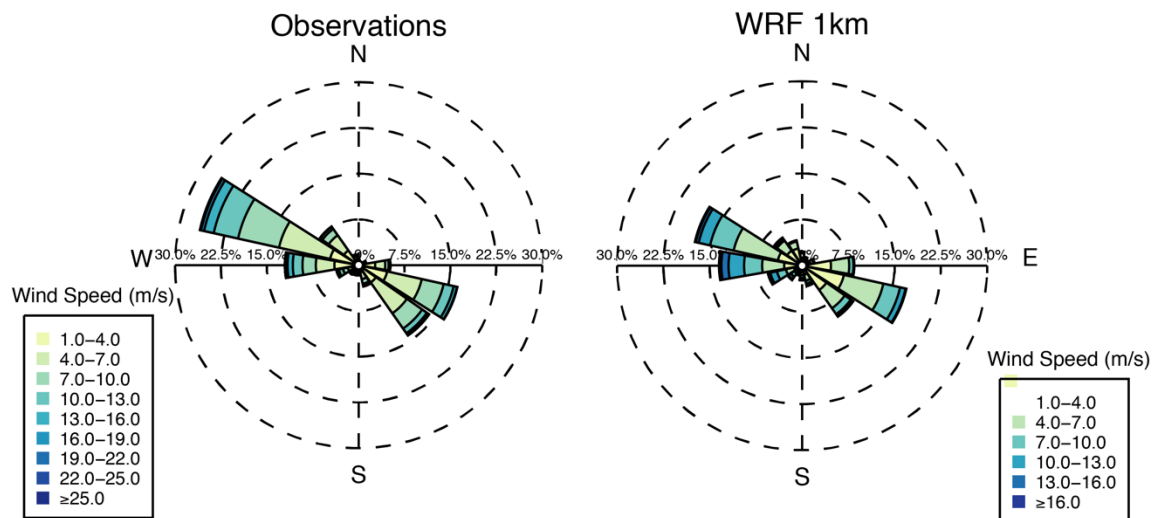
Figure 7: Wind rose of simulated and observed 10 wind speed and direction at Finse AWS stations for the entire simulation period.

690
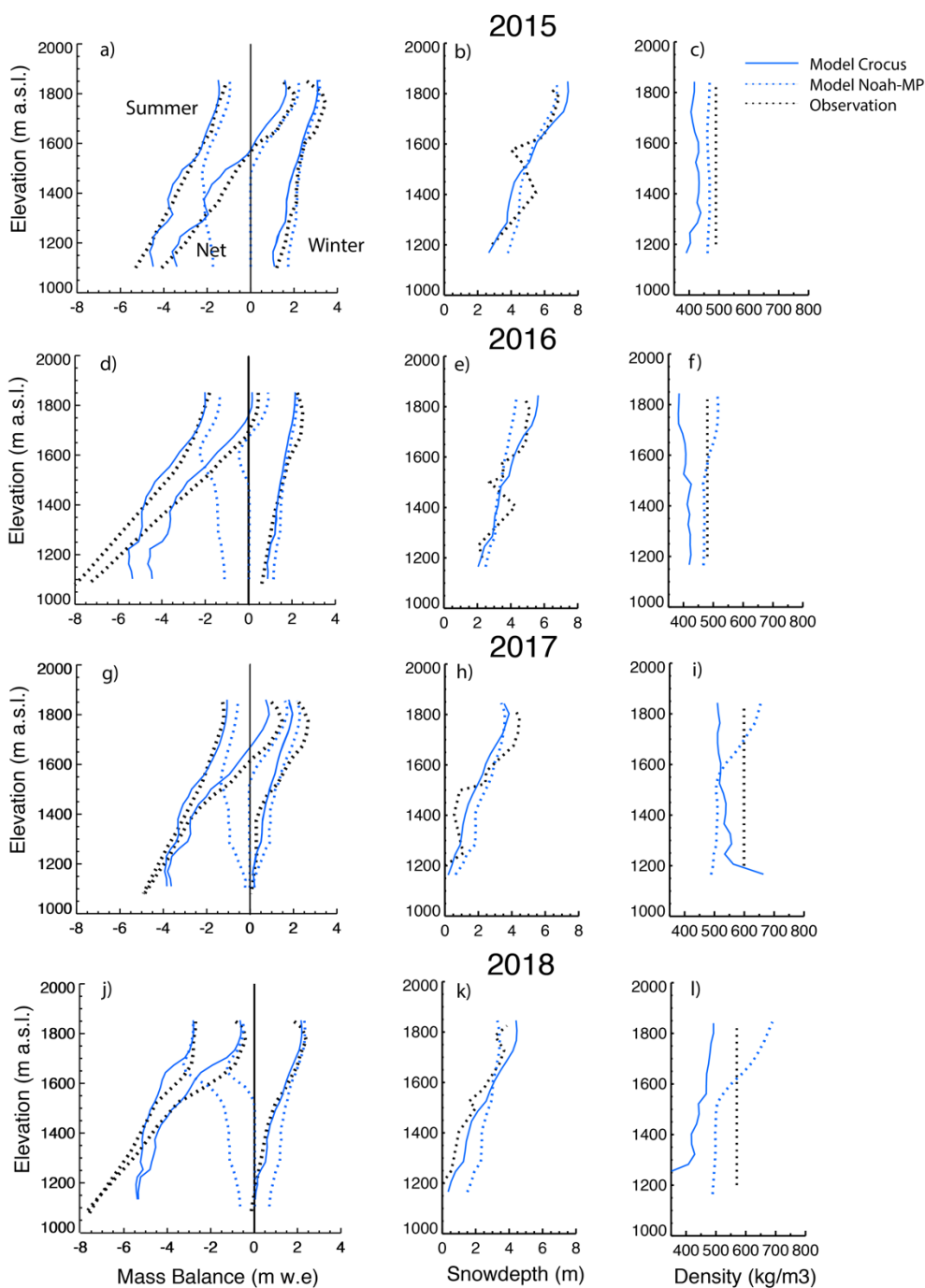
Figure 8: Left panels: Mass balance across Rembesdalskåka with height (a, d, g and j). Middle panel (b, e, h and k): Accumulated snow thickness associated with the winter mass balance. Right panel (c, f, I and l): Snow density of the accumulated snow. Each row represents a different year.

695
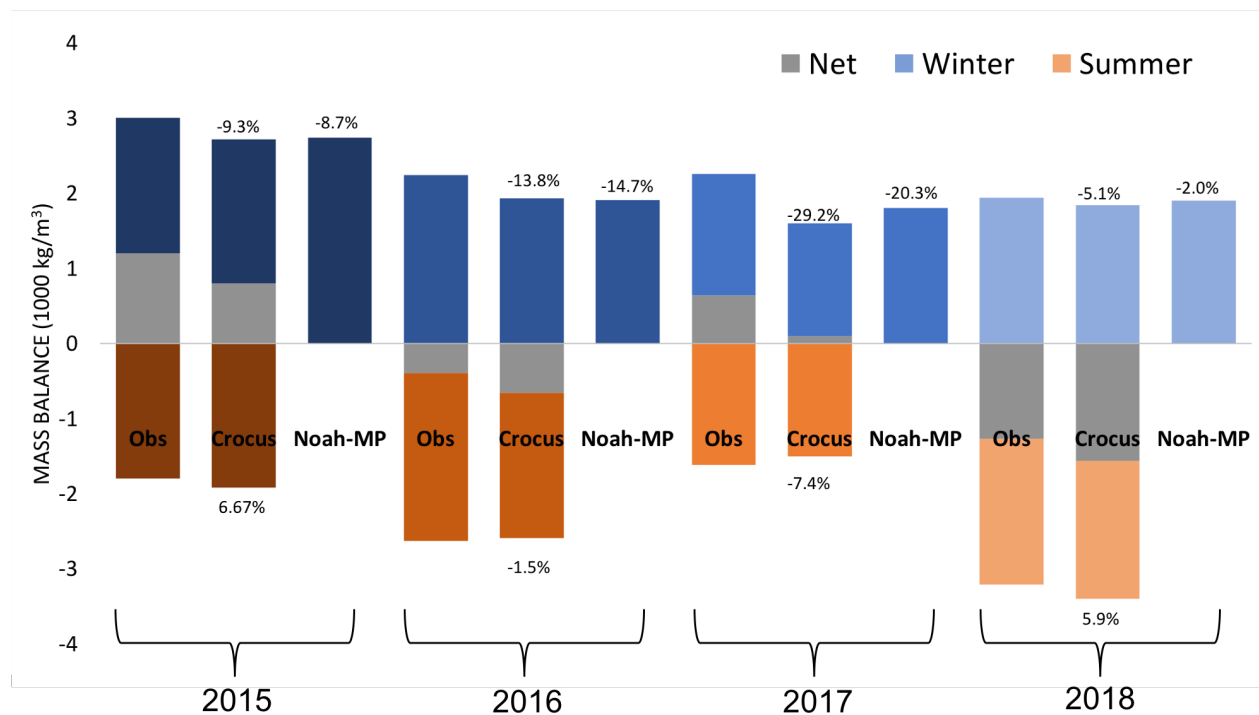
Figure 9: Box plot of winter, summer and net balance for the mass balance years 2015-2018 for Rembesdalskåka. Only winter mass balance is shown for Noah-MP.

700
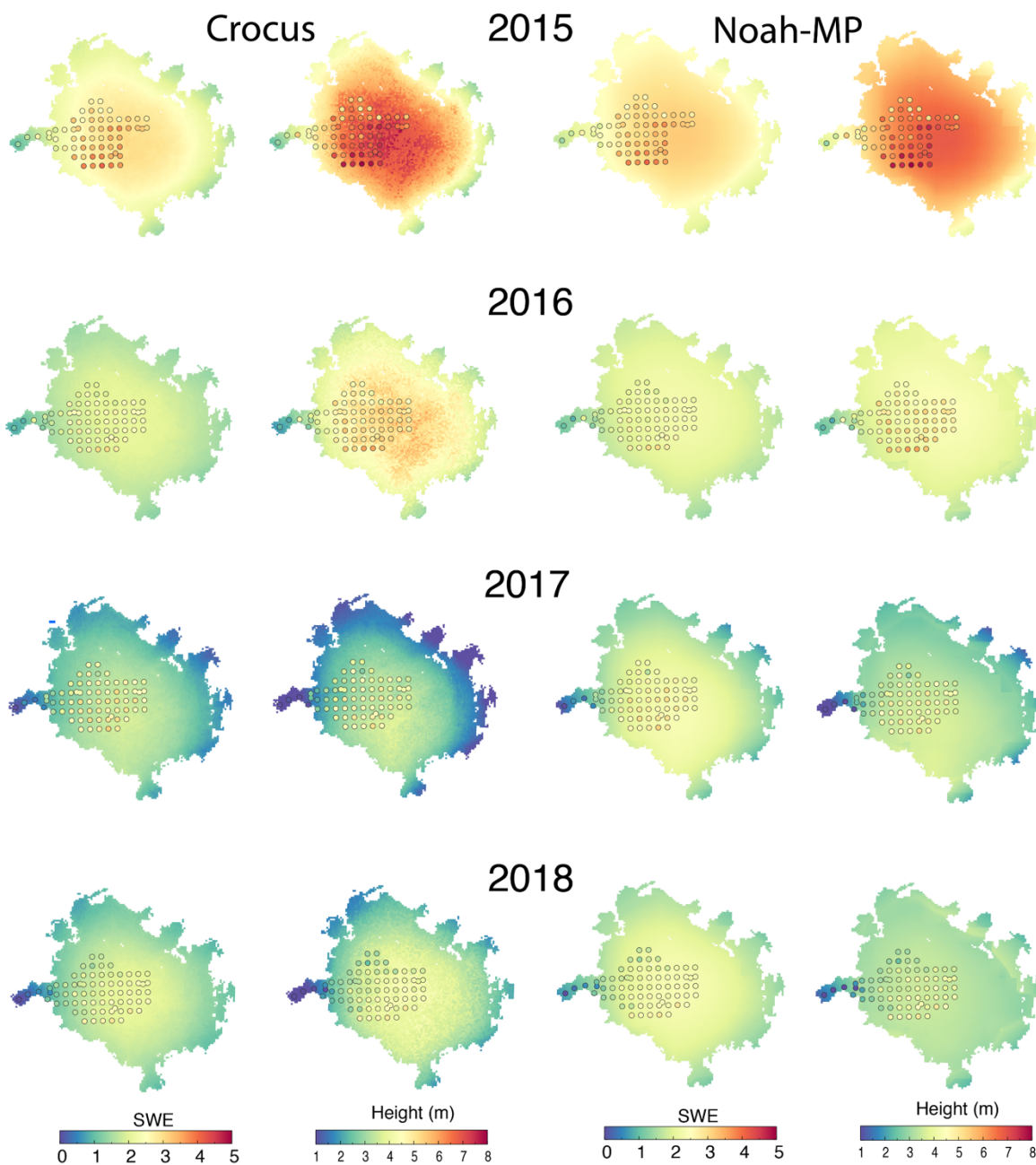
Figure 10: Mass balance at Rembesdalskåka. Two left panels: Winter mass balance and accumulated snow height across Hardangerjøkulen as modeled with Crocus. Colored circles are observations from NVE. Two right panels: Same as the two left panels but as modeled with Noah-MP
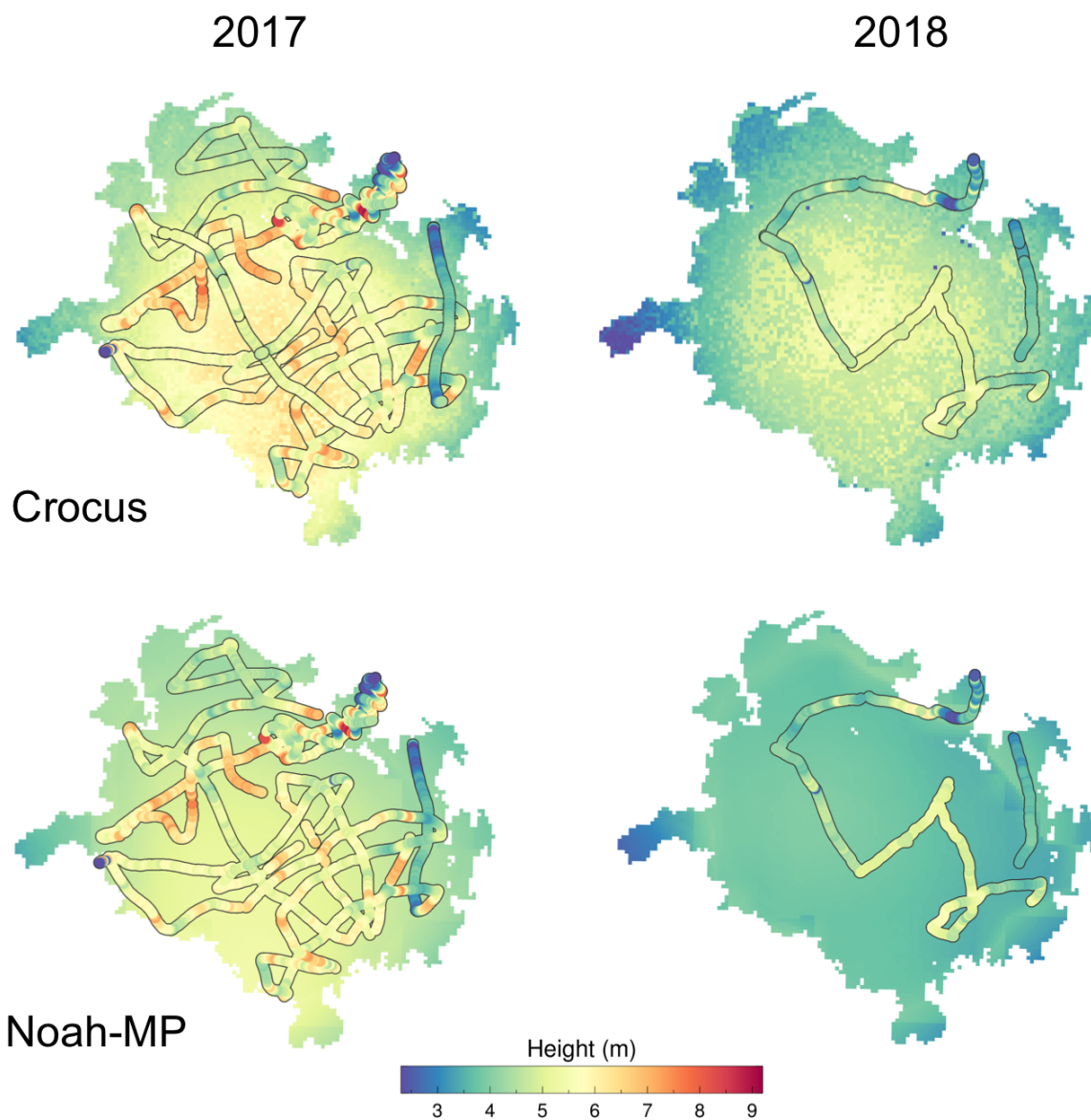
710

Figure 11: Modeled and observed snow accumulation in April. Observations are with Ground Penetrating Radar. Top plots are simulation results with Crocus and bottom plots are simulation results with Noah-MP.
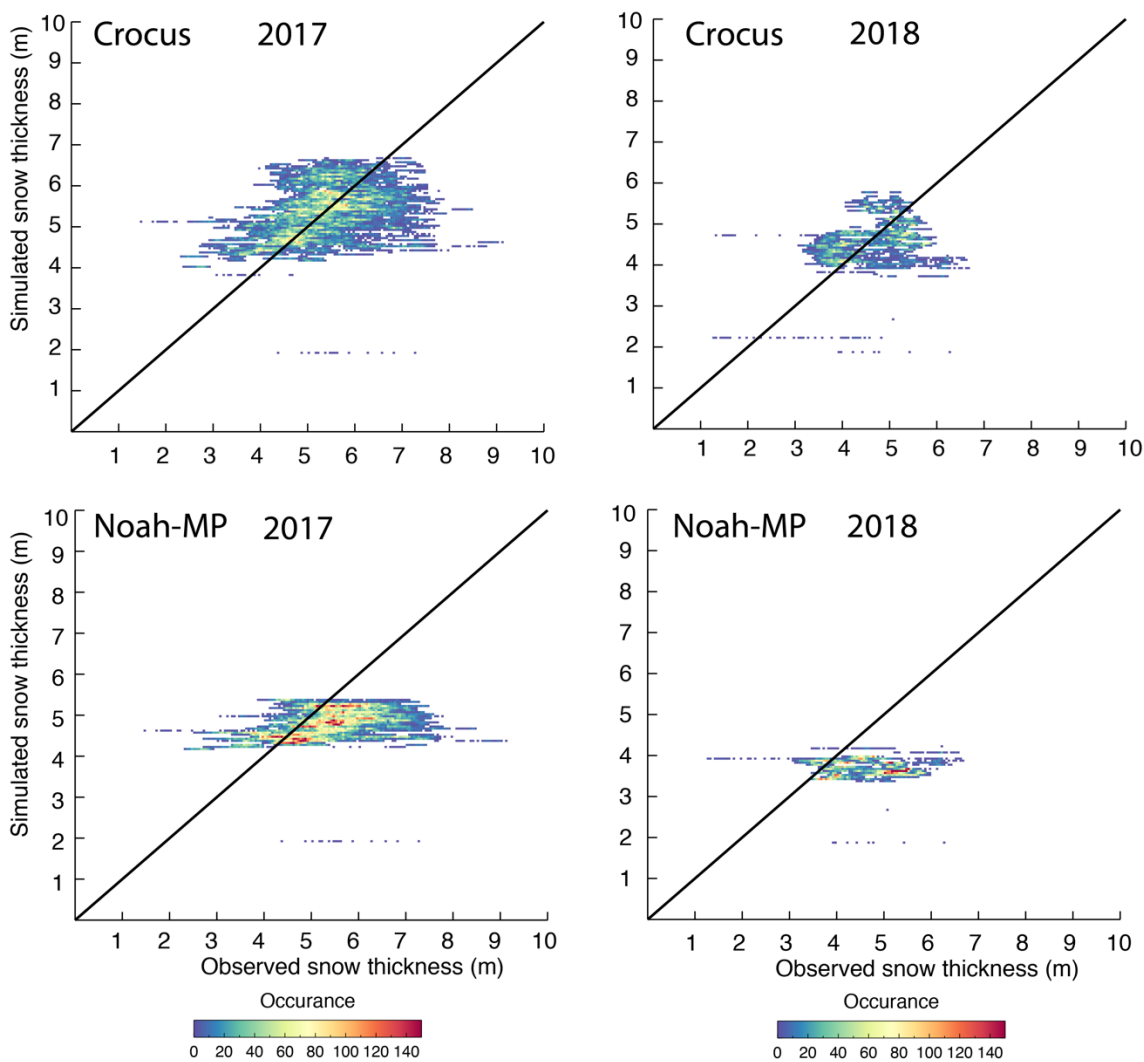
715

Figure 12: Scatter plot of modeled and observed snow accumulation. The observations are with Ground Penetrating Radar. Top plots are simulation results with Crocus and bottom plots are simulation results with Noah-MP.
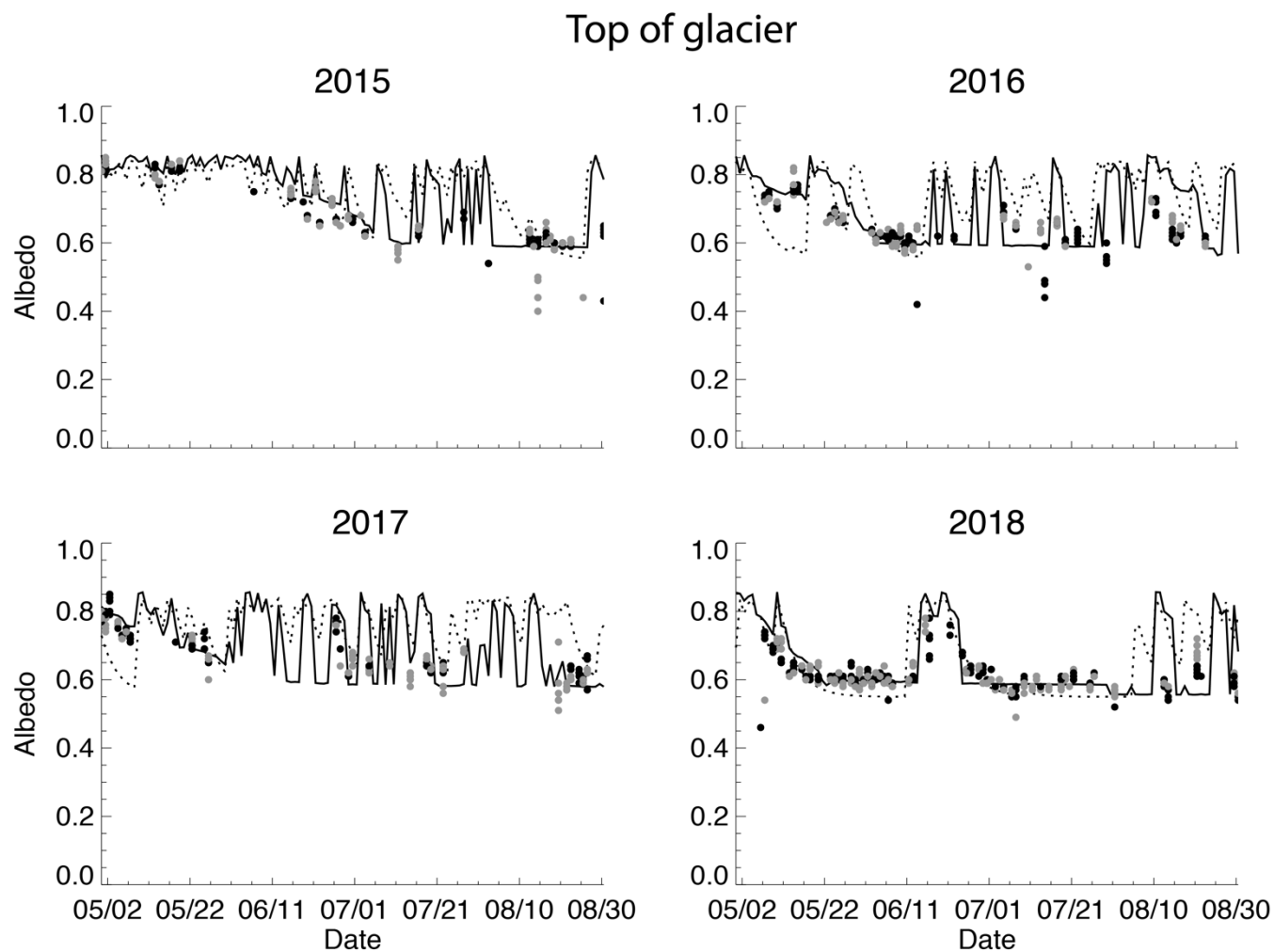
Figure 13: Observed and modeled albedo at the top of Hardangerjøkulen. Dots represent observed albedo from the MODIS satellite (Grey: Terra, Black: Aqua). Solid line is albedo from the Crocus snow model, dashed line is albedo from the Noah-MP snow model.
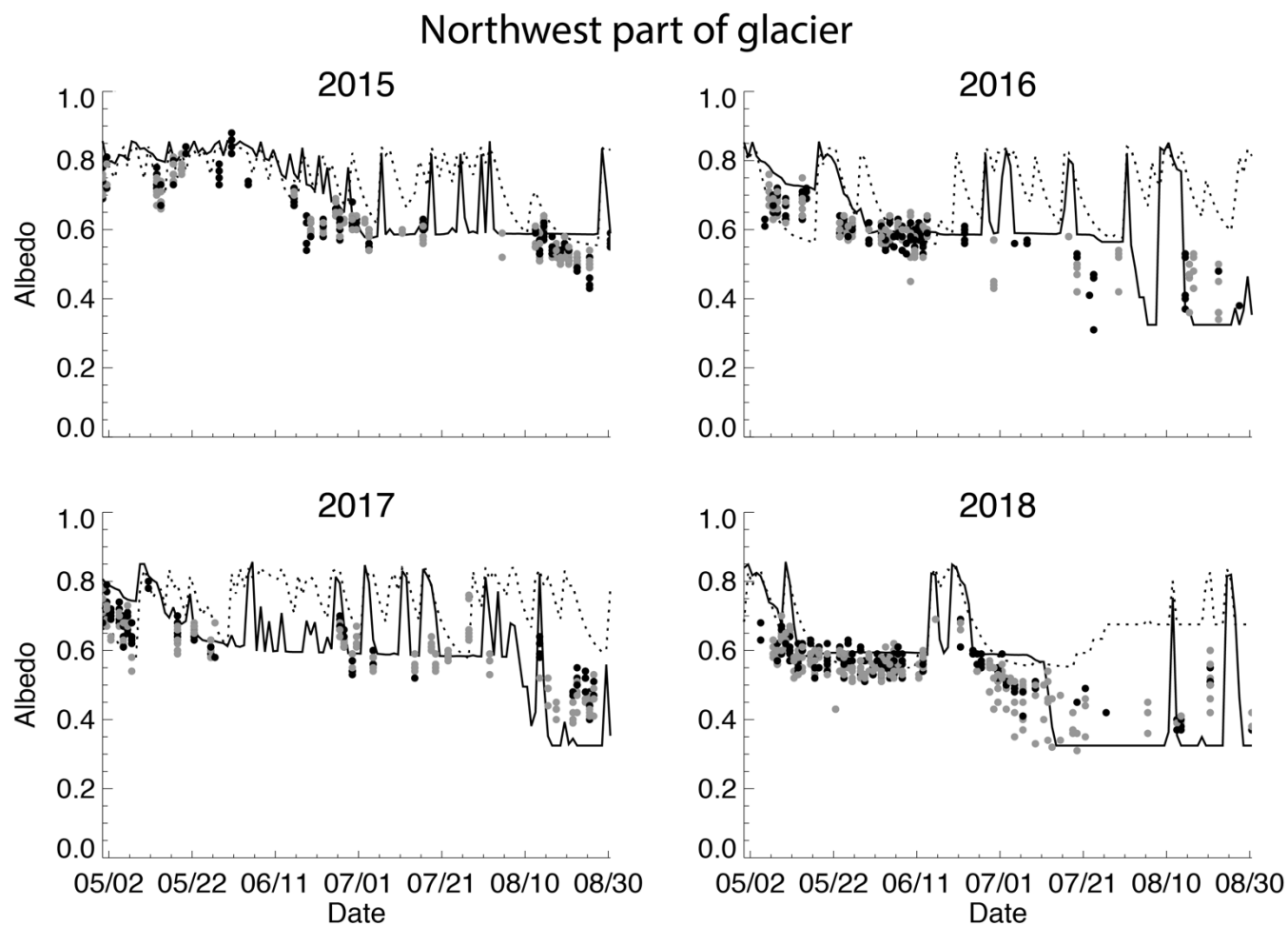
725

Figure 14: Same as Fig. 13 but at a Northwest part of Hardangerjøkulen, where snow at times completely melts to the ice surface.
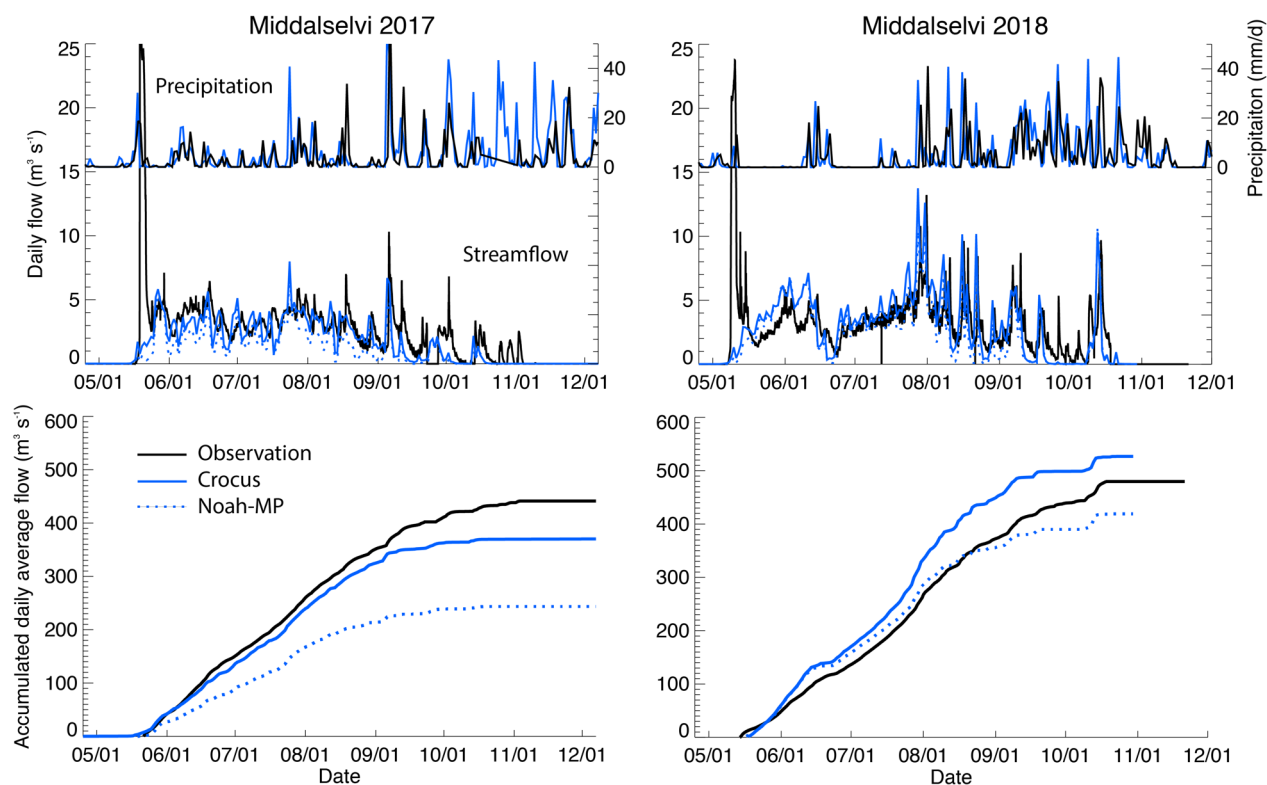
730

Figure 15: Top: Observed (black line) and modeled (blue) precipitation at the Finse AWS station and daily discharge at Midtdalselvi.
Bottom: Accumulated discharge. Solid blue line is with Crocus and dashed blue line is with Noah-MP.

735
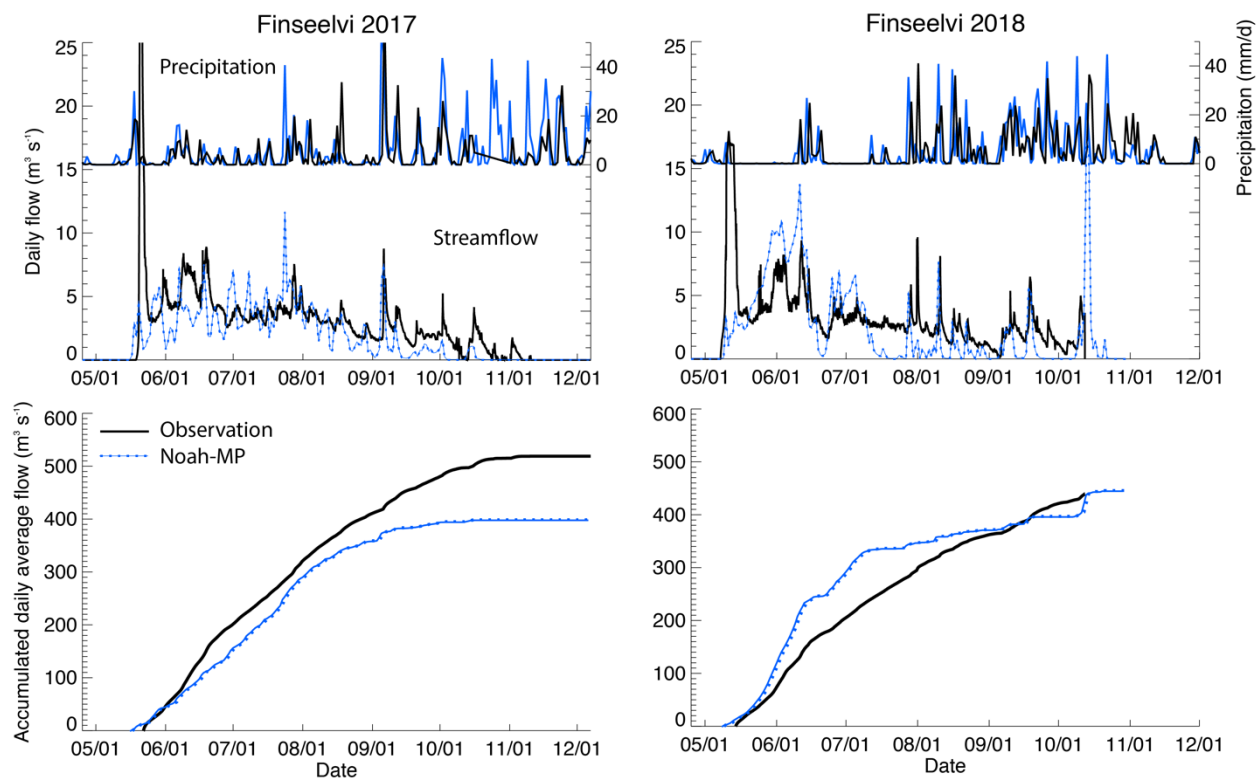
Figure 16: Same as Fig. 15, but for Finseelvi. Note that in this watershed, the WRF-Hydro/Glacier system is not using Crocus, but
740 **Noah-MP due to lack of glaciers.**

745

750

755
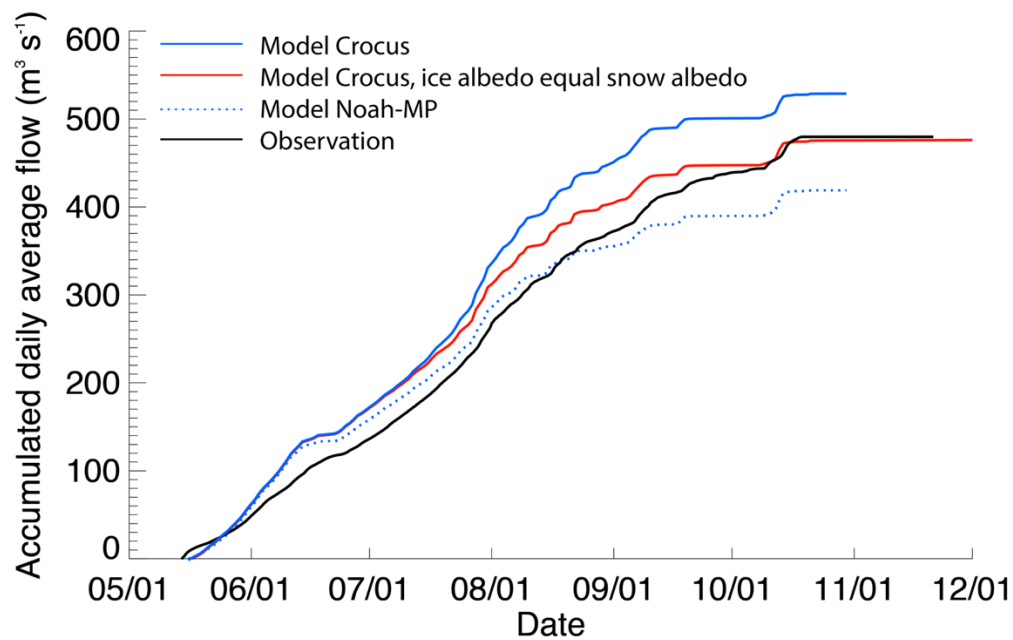
Figure 17: Accumulated stream flow at Middalselvi in 2018. Red is the sensitivity test where snow albedo is used instead of ice albedo.